IEEE Access
Multidisciplinary ⋮ Rapid Review ⋮ Open Access Journal

Received July 24, 2019, accepted August 15, 2019, date of publication August 26, 2019, date of current version September 6, 2019.

Digital Object Identifier 10.1109/ACCESS.2019.2937631

Performance Analysis of Physical-Layer Security Over Fluctuating Beckmann Fading Channels

HUSSIEN AL-HMOOD[1], **(Member, IEEE), AND**
HAMED AL-RAWESHIDY[2], **(Senior Member, IEEE)**
[1]Electrical and Electronic Engineering (EEE) Department, University of Thi-Qar, Thi-Qar 0096442, Iraq
[2]Electrical and Computer Engineering (ECE) Department, College of Engineering, Design and Physical Sciences, Brunel University London, Uxbridge UB8 3PH, U.K.

Corresponding author: Hussien Al-Hmood (hussien.al-hmood@brunel.ac.uk)

ABSTRACT In this paper, we analyse the performance of physical layer security over Fluctuating Beckmann (FB) fading channel, which is an extended model of both the $\kappa - \mu$ shadowed and the classical Beckmann distributions. Specifically, the average secrecy capacity (ASC), secure outage probability (SOP), the lower bound of SOP (SOP^L), and the probability of strictly positive secrecy capacity (SPSC) are derived using two different values of the fading parameters, namely, m and μ which represent the multipath and shadowing severity impacts, respectively. Firstly, when the fading parameters are arbitrary values, the performance metrics are derived in exact expressions in terms of the extended generalised bivariate Fox's H-function (EGBFHF) that has been widely implemented in the open literature. In the second case, to obtain simple mathematically tractable expressions in terms of analytic functions as well as to gain more insight on the behaviour of the physical layer security over Fluctuating Beckmann fading channel models, m and μ are assumed to be integer and even numbers, respectively. In addition, the asymptotic behaviour for all the studied performance metrics has been provided. The numerical results of this analysis are verified via Monte Carlo simulations.

INDEX TERMS Fluctuating Beckmann fading channel, average secrecy capacity, secure outage probability, probability of strictly positive secrecy capacity.

I. INTRODUCTION

Shannon's information-theoretic notion of perfect secrecy has been developed by Wyner using the wiretap channel [1]. In the notion of this channel, an eavesdropper is presented when a legitimate user, namely, Alice, communicates in secrecy with the intended receiver, which is called Bob. The performance of the physical layer security over different fading channel models has been widely analysed in the open literature. For instance, the probability of strictly positive secrecy capacity (SPSC), the secure outage probability (SOP), and the average secrecy capacity (ASC) when the wireless channels subject to the additive white Gaussian noise (AWGN) and Rayleigh fading channel are given in [2] and [3], respectively. In [4], the SPSC when both the main and eavesdropper channels undergo Rician fading channel is derived. The SOP and the SPSC of the physical layer using Rician and Nakagami-m fading conditions for the Bob and the eavesdropper wireless channels are given in [5]. The Weibull fading channel model is used in [6] and [7] to study the SPSC and ASC, respectively.

Recently, many works have been implemented using various generalized fading distributions that unify most of the well-known channel models. In addition, they provide results closer to the practical data than the conventional distributions, namely, Rayleigh, Nakagami-m, and Nakagami-n. In [8], the ASC over $\kappa - \mu$ fading channel that is used to model the line-of-sight (LoS) communication environment is derived. The performance of the physical layer security in non-linear communication scenario is analysed in 9] and [10] via utilising the $\alpha - \mu$ fading condition. Moreover, the ASC, the SOP, the SOP^L, and the SPSC of the physical layer over $\alpha - \mu$ fading using the Fox's H-function channel model, which is a unified framework for a variety of distributions, are presented in [11]. The ASC using the $\kappa - \mu/\alpha - \mu$ and $\alpha - \mu/\kappa - \mu$ fading scenarios for the main/eavesdropper channels is given in [12]. The more generalised fading channels $\alpha - \kappa - \mu$ and $\alpha - \eta - \mu$ are used in [13] to derive the SOP^L and its

The associate editor coordinating the review of this article and approving it for publication was Safdar Hussain Bouk.

asymptotic value. These fading distributions are provided in a single model which is $\alpha - \eta - \kappa - \mu$ that is also used to represent both the main channel and the eavesdropper's channel of the classic Wyner's wiretap model in [14].

The wireless communication channels may also affected by the multipath and shadowing simultaneously. Hence, the performance metrics of the physical layer security over composite fading channels have been also derived by several efforts in the open literature. For example, the analysis in [15]-[17] are investigated over generalised-K (K_G) fading channel, which is a composite of Nakagami-m/gamma distributions using different methods. In [11] and [18], the Fisher-Snedecor $\mathcal{F}$ distribution that is proposed as an alternative approach for the K_G fading condition via employing the inverse Nakagami-m distribution instead of gamma model is used to derive the expression of the ASC, the SOP, the SOP^L, and the SPSC of the physical layer. The ASC and the SOP over $\kappa - \mu$ shadowed fading are given in [19] for integer fading parameters as well as in terms of the derivative of the incomplete moment generating function IMGF) framework that is included a bivariate confluent hypergeometric function $\Phi_2(.)$. This channel model is also utilised in [20] to analyse the SOP^L and SPSC using the exact probability density function (PDF) and the Gamma distribution as an approximate approach. However, the results in both efforts are either included double infinite series or approximated. Therefore, the authors in [21] have extensively analysed the performance of the physical layer security over $\kappa - \mu$ shadowed fading channel using exact closed-form analytic expressions for both scenarios of the values of the fading parameters.

More recent, the so-called Fluctuating Beckmann (FB) fading channel has been proposed as an extended model of the $\kappa - \mu$ shadowed and the classical Beckmann distributions [22]. The FB fading model includes the one-sided Gaussian, Rayleigh, Nakagami-m, Rician, $\kappa - \mu$, $\eta - \mu$, $\eta - \kappa$, Beckmann, Rician shadowed and the $\kappa - \mu$ shadowed distributions as special cases. Hence, the FB fading channel is more generalised than the $\kappa - \mu$ shadowed fading. In addition to [22], the FB fading channel model has been utilised by very few works in the open technical literature [23 and references therein]. This is because its statistical properties are expressed in terms of the multivariate confluent hypergeometric function $\Phi_2(.)$ which is mathematically complicated.

Motivated by the above, this paper is dedicated to analyse the secrecy performance of the physical layer over FB fading channels. Our main contributions are summarised as follows:

- Analysing the performance of the physical layer security when both the main and wiretap channels are subjected to FB fading channel models. In particular, novel exact closed-form mathematically tractable expressions of the ASC, SOP, SOP^L, and SPSC are derived.
- When the fading parameters, namely, μ and m, which represent the real extension of multipath clusters and shadowing severity index, respectively, are arbitrary numbers, the secrecy performance metrics are obtained in terms of the extended generalised bivariate Fox's H-function (EGBFHF). Although, this function is not yet available in the popular mathematical software packages such as MATLAB, MATHEMATICA, and Python, it has been efficiently implemented by various programming codes such as 10], [24] and [25].
- To earn more insights into the behaviour of the physical layer security as well as the impact of the parameters of the FB fading model via using simple exact closed-from analytic expressions of the aforementioned performance metrics, μ and m are assumed to even and integer values. Consequently, the derived results are obtained in simple mathematical functions that are presented in all software packages.
- The asymptotic behaviour for the ASC, SOP, SOP^L and SPSC at high SNR regime is investigated.
- From the provided literature in this work, the ASC, the SOP, the SOP^L, and the SPSC for some special cases of the FB fading model such as Beckmann have not been yet introduced due to the complexity of their PDF and cumulative distribution function (CDF). However, these expressions can be deduced from our derived expressions because the FB fading model is a versatile representation of many distributions such as $\kappa - \mu$ shadowed and Beckmann.

Organization: Section II is divided into two subsections. In the first subsection, the system model that is used in this work is described whereas the general and limited formats of the PDF and the CDF of the instantaneous signal-to-noise ratio (SNR) over FB fading channel are given in the second subsection. The ASC, the SOP, the SOP^L, and the SPSC for two cases of the values of μ and shadowing parameters are derived in Sections III, IV, V, and VI, respectively. Section VII derives the asymptotic expressions of the ASC, the SOP, and the SOP^L at high SNR scenario. The performance of the physical layer security over some special cases of FB fading channels is demonstrated in Section VIII. In Section IX, the Monte Carlo simulations and numerical results are presented. Finally, some conclusions are highlighted in Section IX.

II. SYSTEM AND CHANNEL MODELS

A. SYSTEM MODEL

The Wyner's wiretap channel is comprised of three different nodes with two wireless communication links [1]. The first link is between the transmitter and the legitimate receiver, which are called Alice and Bob, respectively, via main channel. Thus, Bob's channel state information (CSI) can be known by Alice. On the other side, the second wireless communication link describes the wiretap channel between Alice and an external receiver, which is named the eavesdropper, which is named Eve. Accordingly, perfect knowledge of Eve's CSI cannot be assumed at Alice and hence information-theoretic security cannot be guaranteed.

In this paper, the main and wiretap channels are assumed to be independent and subject to quasi-static FB fading. In addition, Alice, Bob, and Eve are equipped with a single antenna and we assume that perfect CSI of the main channel is available at both Bob and Eve. When Alice transmits the signal $s(n)$, the received signals $r_l(n)$ at both Bob and Eve is given as [20]

$$r_l(n) = h_l(n)s(n) + w_l(n). \tag{1}$$

where $l \in \{D, E\}$, D, and E stand for Bob, and eavesdropper, respectively. Moreover, $h_l(n)$ and $w_l(n)$ are the FB fading channel gain and the additive white Gaussian noise (AWGN) assumed to have zero-mean and fixed variance, respectively.

B. THE PDF AND CDF OF FLUCTUATING BECKMANN FADING CHANNEL MODEL

Case_1: The PDF of the instantaneous SNR γ_l, $f_{\gamma_l}(\gamma_l)$, for the destination (Bob), D, and the eavesdropper, E, channels using FB fading channel model is given by [22, eq. (5)]

$$f_{\gamma_l}(\gamma_l) = \frac{\Omega_l}{\Gamma(\mu_l)}\gamma_l^{\mu_l-1}\Phi_2^{(4)}\left(\frac{\mu_l}{2}-m_l, \frac{\mu_l}{2}-m_l, m_l, m_l; \mu_l; -\frac{\gamma_l}{\bar{\gamma}_l\sqrt{\eta_l\alpha_{2_l}}}, -\frac{\gamma_l\sqrt{\eta_l}}{\bar{\gamma}_l\sqrt{\alpha_{2_l}}}, -\frac{\gamma_l c_{1_l}}{\bar{\gamma}_l}, -\frac{\gamma_l c_{2_l}}{\bar{\gamma}_l}\right). \tag{2}$$

where $\Omega_l = \frac{\alpha_{2_l}^{m_l-\frac{\mu_l}{2}}}{\bar{\gamma}_l^{\mu_l}\alpha_{1_l}^{m_l}}$, $\alpha_{2_l} = \frac{4\eta_l}{\mu_l^2(1+\eta_l)^2(1+\kappa_l)^2}$, $\bar{\gamma}_l$ is the average SNR, m_l is the shadowing severity parameter, $\Gamma(a) = \int_0^\infty x^{a-1}e^{-x}dx$ is the Gamma function and $\Phi_2^{(4)}(.)$ is the multivariate confluent hypergeometric function defined in [26, eq. (1.7.10)]. Furthermore, $c_{1l,2l}$ are the roots of $\alpha_{1l}s^2 + \beta_l s + 1$ with

$$\alpha_{1_l} = \alpha_{2_l} + \frac{2\kappa_l(\varrho_l^2+\eta_l)}{m_l(1+\varrho_l^2)\mu_l(1+\eta_l)(1+\kappa_l)^2}.$$
$$\beta_l = -\frac{1}{1+\kappa_l}\left[\frac{2}{\mu_l}+\frac{\kappa_l}{m_l}\right]. \tag{3}$$

where $\kappa_l = \frac{p_l^2+q_l^2}{\mu_l(\sigma_{x_l}^2+\sigma_{y_l}^2)}$, $\varrho_l^2 = \frac{p_l^2}{q_l^2}$, $\eta_l = \frac{\sigma_{x_l}^2}{\sigma_{y_l}^2}$, $\sigma_{x_l}^2 = E[X_{i_l}^2]$, $\sigma_{y_l}^2 = E[Y_{i_l}^2]$, p_{i_l} and q_{i_l} are real numbers for ith cluster and $X_{i_l}^2$ and $Y_{i_l}^2$ mutually independent Gaussian random processes.

The CDF of the FB fading channel condition is expressed as [22, eq. (6)]

$$F_{\gamma_l}(\gamma_l) = \frac{\Omega_l}{\Gamma(\mu_l+1)}\gamma_l^{\mu_l}\Phi_2^{(4)}\left(\frac{\mu_l}{2}-m_l, \frac{\mu_l}{2}-m_l, m_l, m_l; \mu_l+1; -\frac{\gamma_l}{\bar{\gamma}_l\sqrt{\eta_l\alpha_{2_l}}}, -\frac{\gamma_l\sqrt{\eta_l}}{\bar{\gamma}_l\sqrt{\alpha_{2_l}}}, -\frac{\gamma_l c_{1_l}}{\bar{\gamma}_l}, -\frac{\gamma_l c_{2_l}}{\bar{\gamma}_l}\right). \tag{4}$$

Case_2: When m is integer value and μ is even number, the PDF and the CDF are, respectively, given by [22, eqs. (10) and (14)]

$$f_{\gamma_l}(\gamma_l) = \Omega_l \sum_{i_l=1}^{N_l(m_l,\mu_l)} e^{-\frac{\vartheta_l}{\bar{\gamma}_l}\gamma_l} \sum_{j_l=1}^{|\omega_{i_l}|} \frac{A_{i_l j_l}}{(j_l-1)!}\gamma_l^{j_l-1}. \tag{5}$$

and

$$F_{\gamma_l}(\gamma_l) = 1 + \Omega_l \sum_{i_l=1}^{N_l(m_l,\mu_l)} e^{-\frac{\vartheta_l}{\bar{\gamma}_l}\gamma_l} \sum_{j_l=1}^{|\omega_{i_l}|} \frac{B_{i_l j_l}}{(j_l-1)!}\gamma_l^{j_l-1}. \tag{6}$$

where $\omega_l = [m_l, m_l, \frac{\mu_l}{2}-m_l, \frac{\mu_l}{2}-m_l]$, $\vartheta_l = [c_{1l}, c_{2l}, \frac{\mu_l(1+\eta_l)(1+\kappa_l)}{2\eta_l}, \frac{\mu_l(1+\eta_l)(1+\kappa_l)}{2}]$, $N_l(m_l,\mu_l) = 2[1 + \mathrm{u}(\frac{\mu_l}{2}, m_l)]$, u(.) is the unit step function, and $A_{i_l j_l}$ and $B_{i_l j_l}$ are calculated by [22, eq.(51)] and [22, eq. (52)], respectively.

III. AVERAGE SECRECY CAPACITY

The normalised ASC that is defined as the difference between the capacity of the main and wiretap channels over instantaneous SNR, γ, can be calculated by $\bar{C}_s = I_1 + I_2 - I_3$ [18, eq. (14)] where I_1, I_2, and I_3 are respectively expressed as

$$I_1 = \int_0^\infty \ln(1+\gamma_D) f_D(\gamma_D) F_E(\gamma_D) d\gamma_D. \tag{7}$$

$$I_2 = \int_0^\infty \ln(1+\gamma_E) f_E(\gamma_E) F_D(\gamma_E) d\gamma_E. \tag{8}$$

$$I_3 = \int_0^\infty \ln(1+\gamma_E) f_E(\gamma_E) d\gamma_E. \tag{9}$$

Theorem 1: The exact mathematically tractable expressions for I_1, I_2, and I_3 using the PDF and the CDF of *Case_1* are given in (10), (11), and (12), as shown at the top of the next page, respectively, where $H_{p,q:c,d;\ldots;d_n,c_n}^{s,r:a,b;\ldots;a_n,b_n}[.]$ denotes the EGBFHF that is defined in [27, A.1]. In this paper, the efficient MATLAB code that is presented in [25] has been employed to compute the EGBFHF. To the best of the authors knowledge, (10), (11), and (12) are novel.

Proof: See Appendix A. ∎

Corollary 1: For *Case_2*, I_1, I_2, and I_3 are respectively derived in simple analytic exact closed-form expressions as follows

$$I_1 = \Omega_D \sum_{i_D=1}^{N_D(m_D,\mu_D)} \sum_{j_D=1}^{|\omega_{i_D}|} \frac{A_{i_D j_D}}{(j_D-1)!} \times \left[\Gamma(j_D)e^{\frac{\vartheta_{i_D}}{\bar{\gamma}_D}} \sum_{k=1}^{j_D} \frac{\Gamma\left(k-j_D, \frac{\vartheta_{i_D}}{\bar{\gamma}_D}\right)}{\left(\frac{\vartheta_{i_D}}{\bar{\gamma}_D}\right)^k} + \Omega_E \sum_{i_E=1}^{N_E(m_E,\mu_E)} \sum_{j_E=1}^{|\omega_{i_E}|} \frac{B_{i_E j_E}\Gamma(j_D+j_E-1)}{(j_E-1)!} e^{\left(\frac{\vartheta_{i_D}}{\bar{\gamma}_D}+\frac{\vartheta_{i_E}}{\bar{\gamma}_E}\right)} \times \sum_{r=1}^{j_D+j_E-1} \frac{\Gamma\left(r-j_D-j_E+1, \frac{\vartheta_{i_D}}{\bar{\gamma}_D}+\frac{\vartheta_{i_E}}{\bar{\gamma}_E}\right)}{\left(\frac{\vartheta_{i_D}}{\bar{\gamma}_D}+\frac{\vartheta_{i_E}}{\bar{\gamma}_E}\right)^{r-j_D-j_E+1}}\right]. \tag{13}$$

$$I_1 = \frac{\Omega_D\Omega_E}{[\Gamma(\frac{\mu_D}{2}-m_D)\Gamma(\frac{\mu_E}{2}-m_E)\Gamma(m_D)\Gamma(m_E)]^2} \times H^{1,2:1,1;1,1;1,1;1,1;1,1;1,1;1,1}_{2,4:1,1;1,1;1,1;1,1;1,1;1,1;1,1}\left[\frac{1}{\bar{\gamma}_D\sqrt{\eta_D\alpha_{2_D}}}, \frac{\sqrt{\eta_D}}{\bar{\gamma}_D\sqrt{\alpha_{2_D}}}, \frac{c_{1_D}}{\bar{\gamma}_D}, \frac{c_{2_D}}{\bar{\gamma}_D}, \frac{1}{\bar{\gamma}_E\sqrt{\eta_E\alpha_{2_E}}}, \frac{\sqrt{\eta_E}}{\bar{\gamma}_E\sqrt{\alpha_{2_E}}}, \frac{c_{1_E}}{\bar{\gamma}_E}, \frac{c_{2_E}}{\bar{\gamma}_E}\right| \begin{matrix}(1-\mu_D-\mu_E;1,1,1,1,1,1,1,1),(1-\mu_D-\mu_E;1,1,1,1,1,1,1,1)\\(-\mu_D-\mu_E;1,1,1,1,1,1,1,1),(1-\mu_D;1,1,1,1,0,0,0,0),(-\mu_E;0,0,0,0,1,1,1,1)\end{matrix}\left|\begin{matrix}(1+m_D-\frac{\mu_D}{2},1)\\(0,1)\end{matrix}\right| \begin{matrix}(1+m_D-\frac{\mu_D}{2},1)\\(0,1)\end{matrix}\left|\begin{matrix}(1-m_D,1)\\(0,1)\end{matrix}\right|\begin{matrix}(1-m_D,1)\\(0,1)\end{matrix}\left|\begin{matrix}(1+m_E-\frac{\mu_E}{2},1)\\(0,1)\end{matrix}\right|\begin{matrix}(1+m_E-\frac{\mu_E}{2},1)\\(0,1)\end{matrix}\left|\begin{matrix}(1-m_E,1)\\(0,1)\end{matrix}\right|\begin{matrix}(1-m_E,1)\\(0,1)\end{matrix}\right]. \quad (10)$$

$$I_2 = \frac{\Omega_E\Omega_D}{[\Gamma(\frac{\mu_E}{2}-m_E)\Gamma(\frac{\mu_D}{2}-m_D)\Gamma(m_E)\Gamma(m_D)]^2} \times H^{1,2:1,1;1,1;1,1;1,1;1,1;1,1;1,1}_{2,4:1,1;1,1;1,1;1,1;1,1;1,1;1,1}\left[\frac{1}{\bar{\gamma}_E\sqrt{\eta_E\alpha_{2_E}}}, \frac{\sqrt{\eta_E}}{\bar{\gamma}_E\sqrt{\alpha_{2_E}}}, \frac{c_{1_E}}{\bar{\gamma}_E}, \frac{c_{2_E}}{\bar{\gamma}_E}, \frac{1}{\bar{\gamma}_D\sqrt{\eta_D\alpha_{2_D}}}, \frac{\sqrt{\eta_D}}{\bar{\gamma}_D\sqrt{\alpha_{2_D}}}, \frac{c_{1_D}}{\bar{\gamma}_D}, \frac{c_{2_D}}{\bar{\gamma}_D}\right| \times \begin{matrix}(1-\mu_E-\mu_D;1,1,1,1,1,1,1,1),(1-\mu_E-\mu_D;1,1,1,1,1,1,1,1)\\(-\mu_E-\mu_D;1,1,1,1,1,1,1,1),(1-\mu_E;1,1,1,1,0,0,0,0),(-\mu_D;0,0,0,0,1,1,1,1)\end{matrix}\left|\begin{matrix}(1+m_E-\frac{\mu_E}{2},1)\\(0,1)\end{matrix}\right| \times \begin{matrix}(1+m_E-\frac{\mu_E}{2},1)\\(0,1)\end{matrix}\left|\begin{matrix}(1-m_E,1)\\(0,1)\end{matrix}\right|\begin{matrix}(1-m_E,1)\\(0,1)\end{matrix}\left|\begin{matrix}(1+m_D-\frac{\mu_D}{2},1)\\(0,1)\end{matrix}\right|\begin{matrix}(1+m_D-\frac{\mu_D}{2},1)\\(0,1)\end{matrix}\left|\begin{matrix}(1-m_D,1)\\(0,1)\end{matrix}\right|\begin{matrix}(1-m_D,1)\\(0,1)\end{matrix}\right]. \quad (11)$$

$$I_3 = \frac{\Omega_E}{[\Gamma(\mu_E-m_E)\Gamma(m_E)]^2} H^{1,2:1,1;1,1;1,1;1,1}_{2,3:1,1;1,1;1,1;1,1}\left[\frac{1}{\bar{\gamma}_E\sqrt{\eta_E\alpha_{2_E}}}, \frac{\sqrt{\eta_E}}{\bar{\gamma}_E\sqrt{\alpha_{2_E}}}, \frac{c_{1_E}}{\bar{\gamma}_E}, \frac{c_{2_E}}{\bar{\gamma}_E}\right| \times \begin{matrix}(1-\mu_E,1),(1-\mu_E,1)\\(1-\mu_E,1),(-\mu_E,1),(-\mu_E,1)\end{matrix}\left|\begin{matrix}(1+m_E-\frac{\mu_E}{2},1)\\(0,1)\end{matrix}\right| \begin{matrix}(1+m_E-\frac{\mu_E}{2},1)\\(0,1)\end{matrix}\left|\begin{matrix}(1-m_E,1)\\(0,1)\end{matrix}\right|\begin{matrix}(1-m_E,1)\\(0,1)\end{matrix}\right]. \quad (12)$$

$$\bar{C}_s = \Omega_D \sum_{i_D=1}^{N_D(m_D,\mu_D)}\sum_{j_D=1}^{|\omega_{i_D}|} A_{i_Dj_D} e^{\frac{\vartheta_{i_D}}{\bar{\gamma}_D}} \sum_{k=1}^{j_D} \frac{\Gamma\left(k-j_D,\frac{\vartheta_{i_D}}{\bar{\gamma}_D}\right)}{\left(\frac{\vartheta_{i_D}}{\bar{\gamma}_D}\right)^k} + \Omega_D\Omega_E \sum_{i_D=1}^{N_D(m_D,\mu_D)}\sum_{j_D=1}^{|\omega_{i_D}|}\sum_{i_E=1}^{N_E(m_E,\mu_E)}\sum_{j_E=1}^{|\omega_{i_E}|} \frac{\Gamma(j_D+j_E-1)}{\Gamma(j_E)\Gamma(j_D)} \times\{A_{i_Dj_D}B_{i_Ej_E}+A_{i_Ej_E}B_{i_Dj_D}\}e^{\left(\frac{\vartheta_{i_D}}{\bar{\gamma}_D}+\frac{\vartheta_{i_E}}{\bar{\gamma}_E}\right)} \sum_{r=1}^{j_D+j_E-1} \frac{\Gamma\left(r-j_D-j_E+1,\frac{\vartheta_{i_D}}{\bar{\gamma}_D}+\frac{\vartheta_{i_E}}{\bar{\gamma}_E}\right)}{\left(\frac{\vartheta_{i_D}}{\bar{\gamma}_D}+\frac{\vartheta_{i_E}}{\bar{\gamma}_E}\right)^{r-j_D-j_E+1}}. \quad (16)$$

$$I_2 = \Omega_E \sum_{i_E=1}^{N_E(m_E,\mu_E)}\sum_{j_E=1}^{|\omega_{i_E}|} \frac{A_{i_Ej_E}}{(j_E-1)!} \times\left[\Gamma(j_E)e^{\frac{\vartheta_{i_E}}{\bar{\gamma}_E}} \sum_{k=1}^{j_E} \frac{\Gamma\left(k-j_E,\frac{\vartheta_{i_E}}{\bar{\gamma}_E}\right)}{\left(\frac{\vartheta_{i_E}}{\bar{\gamma}_E}\right)^k} + \Omega_D \sum_{i_D=1}^{N_D(m_D,\mu_D)}\sum_{j_D=1}^{|\omega_{i_D}|} \frac{B_{i_Dj_D}\Gamma(j_E+j_D-1)}{(j_D-1)!}e^{\left(\frac{\vartheta_{i_E}}{\bar{\gamma}_E}+\frac{\vartheta_{i_D}}{\bar{\gamma}_D}\right)} \times \sum_{r=1}^{j_E+j_D-1} \frac{\Gamma\left(r-j_E-j_D+1,\frac{\vartheta_{i_E}}{\bar{\gamma}_E}+\frac{\vartheta_{i_D}}{\bar{\gamma}_D}\right)}{\left(\frac{\vartheta_{i_E}}{\bar{\gamma}_E}+\frac{\vartheta_{i_D}}{\bar{\gamma}_D}\right)^{r-j_E-j_D+1}}\right]. \quad (14)$$

$$I_3 = \Omega_E \sum_{i_E=1}^{N_E(m_E,\mu_E)}\sum_{j_E=1}^{|\omega_{i_E}|} A_{i_Ej_E} e^{\frac{\vartheta_{i_E}}{\bar{\gamma}_E}} \times \sum_{k=1}^{j_E} \frac{\Gamma\left(k-j_E,\frac{\vartheta_{i_E}}{\bar{\gamma}_E}\right)}{\left(\frac{\vartheta_{i_E}}{\bar{\gamma}_E}\right)^k}. \quad (15)$$

Proof: See Appendix B. ■

Substituting (13), (14), and (15) into $\bar{C}_s = I_1 + I_2 - I_3$ and performing some straightforward algebraic manipulations, novel result is obtained as shown in (16), as shown at the top of this page.

IV. SECURE OUTAGE PROBABILITY

The SOP is defined as the probability of the instantaneous secrecy capacity, C_s, falling below the target secrecy threshold, R_s, i.e., $\mathcal{P}(C_s < R_s)$, where $\mathcal{P}(.)$ stands for the probability. Mathematically, the SOP can be evaluated by [15, eq. (24)]

$$\text{SOP} = \int_0^\infty F_D(\theta\gamma_E+\theta-1) f_E(\gamma_E) d\gamma_E. \quad (17)$$

where $\theta = \exp(R_s) \geq 1$ with $R_s \geq 0$ denotes the target secrecy threshold.

Theorem 2: The SOP for *Case*_1 and *Case*_2 are expressed in exact format as given in (18) and (19), as shown at the top of the next page, respectively, at the top of this page. In (19), $\binom{b}{a} \triangleq \frac{b!}{(b-a)!}$ stands for the binomial coefficient [26, eq. (1.1.16)] and $(a)_r$ is the Pochhammer symbol [26, eq. (1.1.15)]. Additionally, (19) is closed-form and simple in comparison with (18) and hence better insights can be obtained for the SOP. To the best authors' knowledge, (18) and (19) are novel and mathematically tractable.

Proof: See Appendix C. ■

$$\text{SOP} = \frac{\Omega_E \Omega_D (\theta-1)^{\mu_D+\mu_E}}{\theta^{\mu_E}[\Gamma(\frac{\mu_E}{2}-m_E)\Gamma(\frac{\mu_D}{2}-m_D)\Gamma(m_E)\Gamma(m_D)]^2} \times H^{1,1:1,1;1,1;1,1;1,1;1,1;1,1;1,1;1,1}_{2,3:1,1;1,1;1,1;1,1;1,1;1,1;1,1;1,1} \left[\frac{\theta-1}{\theta\bar{\gamma}_E\sqrt{\eta_E\alpha_{2_E}}}, \frac{(\theta-1)\sqrt{\eta_E}}{\theta\bar{\gamma}_E\sqrt{\alpha_{2_E}}}, \frac{(\theta-1)c_{1_E}}{\theta\bar{\gamma}_E}, \frac{(\theta-1)c_{2_E}}{\theta\bar{\gamma}_E}, \frac{\theta-1}{\bar{\gamma}_D\sqrt{\eta_D\alpha_{2_D}}}, \frac{(\theta-1)\sqrt{\eta_D}}{\bar{\gamma}_D\sqrt{\alpha_{2_D}}}, \frac{(\theta-1)c_{1_D}}{\bar{\gamma}_D}, \frac{(\theta-1)c_{2_D}}{\bar{\gamma}_D} \middle| \begin{matrix} (1-\mu_E;1,1,1,1,0,0,0,0),(-\mu_D;0,0,0,0,1,1,1,1) \\ (-\mu_E-\mu_D;1,1,1,1,1,1,1,1),(-\mu_E;1,1,1,1,0,0,0,0),(-\mu_D;0,0,0,0,1,1,1,1) \end{matrix} \middle| (1+m_E-\frac{\mu_E}{2},1) \middle| (0,1) \times \begin{matrix} (1+m_E-\frac{\mu_E}{2},1) \\ (0,1) \end{matrix} \middle| \begin{matrix} (1-m_E,1) \\ (0,1) \end{matrix} \middle| \begin{matrix} (1-m_E,1) \\ (0,1) \end{matrix} \middle| \begin{matrix} (1+m_D-\frac{\mu_D}{2},1) \\ (0,1) \end{matrix} \middle| \begin{matrix} (1+m_D-\frac{\mu_D}{2},1) \\ (0,1) \end{matrix} \middle| \begin{matrix} (1-m_D,1) \\ (0,1) \end{matrix} \middle| \begin{matrix} (1-m_D,1) \\ (0,1) \end{matrix} \right]. \tag{18}$$

$$\text{SOP} = 1 + \Omega_D\Omega_E \sum_{i_E=1}^{N_E(m_E,\mu_E)} \sum_{j_E=1}^{|\omega_{i_E}|} A_{i_E j_E} \sum_{i_D=1}^{N_D(m_D,\mu_D)} \sum_{j_D=1}^{|\omega_{i_D}|} \frac{B_{i_D j_D}}{\Gamma(j_D)} e^{\frac{\vartheta_{i_D}}{\bar{\gamma}_D}(1-\theta)} \times \sum_{r=0}^{j_D-1} \binom{j_D-1}{r} \frac{\theta^r (j_E)_r}{(\theta-1)^{r-j_D+1}\left(\frac{\theta\vartheta_{i_D}}{\bar{\gamma}_D}+\frac{\vartheta_{i_E}}{\bar{\gamma}_E}\right)^{r+j_E}}. \tag{19}$$

$$\text{SOP}^L = \frac{\Omega_E\Omega_D\theta^{\mu_D}}{\phi^{\mu_E+\mu_D}\Gamma(\frac{\mu_E}{2}-m_E)\Gamma(\frac{\mu_D}{2}-m_D)[\Gamma(m_E)\Gamma(m_D)]^2} \times H^{0,1:1,1;1,1;1,1;1,1;1,1;1,1;1,1;1,1}_{1,2:1,1;1,1;1,1;1,1;1,1;1,1;1,1;1,1} \left[\frac{\eta_E-1}{\phi\bar{\gamma}_E\sqrt{\eta_E\alpha_{2_E}}}, \frac{\sqrt{\eta_E\alpha_{2_E}}c_{1_E}-1}{\phi\bar{\gamma}_E\sqrt{\eta_E\alpha_{2_E}}}, \frac{\sqrt{\eta_E\alpha_{2_E}}c_{2_E}-1}{\phi\bar{\gamma}_E\sqrt{\eta_E\alpha_{2_E}}}, \frac{(\eta_D-1)\theta}{\phi\bar{\gamma}_D\sqrt{\eta_D\alpha_{2_D}}}, \frac{(\sqrt{\eta_D\alpha_{2_D}}c_{1_D}-1)\theta}{\phi\bar{\gamma}_D\sqrt{\eta_D\alpha_{2_D}}}, \frac{(\sqrt{\eta_D\alpha_{2_D}}c_{2_D}-1)\theta}{\phi\bar{\gamma}_D\sqrt{\eta_D\alpha_{2_D}}} \middle| \begin{matrix} (1-\mu_D-\mu_E;1,1,1,1,1,1) \\ (1-\mu_E;1,1,1,0,0,0),(-\mu_D;0,0,0,1,1,1) \end{matrix} \middle| (1+m_E-\frac{\mu_E}{2},1) \middle| (0,1) \middle| \begin{matrix} (1-m_E,1) \\ (0,1) \end{matrix} \middle| \begin{matrix} (1+m_D-\frac{\mu_D}{2},1) \\ (0,1) \end{matrix} \middle| \begin{matrix} (1-m_D,1) \\ (0,1) \end{matrix} \middle| \begin{matrix} (1-m_D,1) \\ (0,1) \end{matrix} \right]. \tag{21}$$

V. LOWER BOUND OF SOP

According to [15], the SOP^L can be obtained from (17) when γ_E tends to ∞. Consequently, the SOP^L can be computed by [15, eq. (27)]

$$\begin{aligned} \text{SOP}^L &= \int_0^\infty F_D(\theta\gamma_E) f_E(\gamma_E) d\gamma_E. \\ &\leq \text{SOP} \end{aligned} \tag{20}$$

Theorem 3: The SOP^L when μ_l and m_l are arbitrary numbers, namely, *Case*_1, is presented in (21), as shown at the top of this page, with $\phi = \frac{\theta}{\bar{\gamma}_D\sqrt{\eta_D\alpha_{2_D}}} + \frac{1}{\bar{\gamma}_E\sqrt{\eta_E\alpha_{2_E}}}$ whereas for *Case*_2, the SOP^L is given as

$$\text{SOP}^L = 1 + \Omega_E\Omega_D \sum_{i_E=1}^{N_E(m_E,\mu_E)} \sum_{j_E=1}^{|\omega_{i_E}|} \frac{A_{i_E j_E}}{\Gamma(j_E)} \times \sum_{i_D=1}^{N_D(m_D,\mu_D)} \sum_{j_D=1}^{|\omega_{i_D}|} \theta^{j_D-1} \frac{\Gamma(j_D+j_E-1)B_{i_D j_D}}{\Gamma(j_D)\left(\frac{\theta\vartheta_{i_D}}{\bar{\gamma}_D}+\frac{\vartheta_{i_E}}{\bar{\gamma}_E}\right)^{j_D+j_E-1}}. \tag{22}$$

Proof: See Appendix D. ■

To the best of our knowledge, (21) and (22) are new. It is evident that (22) is obtained in simple exact closed-form expression.

VI. PROBABILITY OF STRICTLY POSITIVE SECRECY CAPACITY

The SPSC refers to the probability of positive C_s, namely, $\mathcal{P}(C_s > 0)$. Therefore, it can be calculated by [8, eq. (19)]

$$\text{SPSC} = 1 - \text{SOP}^L. \quad \text{for} \quad \theta = 1 \tag{23}$$

It can be observed that the SPSC for *Case*_1 and *Case*_2 can be obtained from (21) and (22), respectively, via substituting $\theta = 1$ and plugging the results in (23).

VII. ASYMPTOTIC ANALYSIS AT HIGH SNR VALUE

To gain more insight into the behaviour of the physical layer security over FB fading channels when the μ and m are arbitrary numbers, the asymptotic analysis at high SNR regime, i.e., $\bar{\gamma}_D \to \infty$ has been studied in this section.

A. ASYMPTOTIC ANALYSIS OF ASC

Theorem 4: The asymptotic expression of ASC, $\bar{C}_s^{Asy}$, over FB fading condition when $\bar{\gamma}_D \to \infty$ is expressed as

$$\bar{C}_s^{Asy} \approx I_1^{Asy} + I_2^{Asy} - I_3^{Asy} \tag{24}$$

where I_1^{Asy} and I_2^{Asy} for FB fading channels are given in (25) and (26), respectively, as shown at the top of the next page. Although I_3^{Asy} can be computed by (12) because it

$$I_1^{Asy} = \frac{\Omega_D\Omega_E}{\Gamma(\mu_D)\Gamma(\mu_E+1)}\sum_{n=0}^{\infty}\frac{(1)_n(1)_n}{(2)_n n!}(-1)^n\Gamma(\mu_D+\mu_E+n+1)(\bar{\gamma}_E\sqrt{\eta_E\alpha_{2_E}})^{\mu_D+\mu_E+n+1}$$
$$\times F_D^{(3)}(\mu_D+\mu_E+n+1;\frac{\mu_E}{2}-m_E,m_E,m_E;\mu_E+1;1-\eta_E,1-\sqrt{\eta_E\alpha_{2_E}}c_{1_E},1-\sqrt{\eta_E\alpha_{2_E}}c_{2_E}) \quad (25)$$

$$I_2^{Asy} = \frac{\Omega_D\Omega_E}{\Gamma(\mu_D+1)\Gamma(\mu_E)}\sum_{n=0}^{\infty}\frac{(1)_n(1)_n}{(2)_n n!}(-1)^n\Gamma(\mu_D+\mu_E+n+1)(\bar{\gamma}_E\sqrt{\eta_E\alpha_{2_E}})^{\mu_D+\mu_E+n+1}$$
$$\times F_D^{(3)}(\mu_D+\mu_E+n+1;\frac{\mu_E}{2}-m_E,m_E,m_E;\mu_E;1-\eta_E,1-\sqrt{\eta_E\alpha_{2_E}}c_{1_E},1-\sqrt{\eta_E\alpha_{2_E}}c_{2_E}) \quad (26)$$

$$I_3^{Asy} = \frac{\Omega_E}{\Gamma(\mu_E)}\sum_{n=0}^{\infty}\frac{(1)_n(1)_n}{(2)_n n!}(-1)^n\Gamma(\mu_E+n+1)(\bar{\gamma}_E\sqrt{\eta_E\alpha_{2_E}})^{\mu_E+n+1}$$
$$\times F_D^{(3)}(\mu_E+n+1;\frac{\mu_E}{2}-m_E,m_E,m_E;\mu_E;1-\eta_E,1-\sqrt{\eta_E\alpha_{2_E}}c_{1_E},1-\sqrt{\eta_E\alpha_{2_E}}c_{2_E}) \quad (27)$$

$$\bar{C}_s^{Asy} \approx \frac{\Omega_E}{\Gamma(\mu_E)}\sum_{n=0}^{\infty}\frac{(1)_n(1)_n}{(2)_n n!}(-1)^n(\bar{\gamma}_E\sqrt{\eta_E\alpha_{2_E}})^{\mu_E+n+1}\Bigg\{\Omega_D\frac{\Gamma(\mu_D+\mu_E+n+1)}{\Gamma(\mu_D)}(\bar{\gamma}_E\sqrt{\eta_E\alpha_{2_E}})^{\mu_D}$$
$$\times\Bigg[\frac{F_D^{(3)}(\mu_D+\mu_E+n+1;\frac{\mu_E}{2}-m_E,m_E,m_E;\mu_E+1;1-\eta_E,1-\sqrt{\eta_E\alpha_{2_E}}c_{1_E},1-\sqrt{\eta_E\alpha_{2_E}}c_{2_E})}{\mu_E}$$
$$+\frac{F_D^{(3)}(\mu_D+\mu_E+n+1;\frac{\mu_E}{2}-m_E,m_E,m_E;\mu_E;1-\eta_E,1-\sqrt{\eta_E\alpha_{2_E}}c_{1_E},1-\sqrt{\eta_E\alpha_{2_E}}c_{2_E})}{\mu_D}\Bigg]$$
$$-\Gamma(\mu_E+n+1)F_D^{(3)}(\mu_E+n+1;\frac{\mu_E}{2}-m_E,m_E,m_E;\mu_E;1-\eta_E,1-\sqrt{\eta_E\alpha_{2_E}}c_{1_E},1-\sqrt{\eta_E\alpha_{2_E}}c_{2_E})\Bigg\} \quad (28)$$

$$T_{\bar{C}_s^{Asy}} \leqslant \frac{(-\bar{\gamma}_E\sqrt{\eta_E\alpha_{2_E}})^N}{\Gamma(N+1)}\Bigg\{\Gamma(\mu_D+\mu_E+N+1)_5F_2(\mu_D+\mu_E+N+1,N+1,N+1,1,1,1;N+2,2;-\bar{\gamma}_E\sqrt{\eta_E\alpha_{2_E}})$$
$$\times\Bigg[F_D^{(3)}(\mu_D+\mu_E+N+1;\frac{\mu_E}{2}-m_E,m_E,m_E;\mu_E+1;1-\eta_E,1-\sqrt{\eta_E\alpha_{2_E}}c_{1_E},1-\sqrt{\eta_E\alpha_{2_E}}c_{2_E})$$
$$+F_D^{(3)}(\mu_E+\mu_D+N+1;\frac{\mu_E}{2}-m_E,m_E,m_E;\mu_E;1-\eta_E,1-\sqrt{\eta_E\alpha_{2_E}}c_{1_E},1-\sqrt{\eta_E\alpha_{2_E}}c_{2_E})\Bigg]$$
$$-\Gamma(\mu_E+N+1)_5F_2(\mu_E+N+1,N+1,N+1,1,1,1;N+2,2;-\bar{\gamma}_E\sqrt{\eta_E\alpha_{2_E}})$$
$$\times F_D^{(3)}(\mu_E+N+1;\frac{\mu_E}{2}-m_E,m_E,m_E;\mu_E;1-\eta_E,1-\sqrt{\eta_E\alpha_{2_E}}c_{1_E},1-\sqrt{\eta_E\alpha_{2_E}}c_{2_E})\Bigg\} \quad (29)$$

$$\mathrm{SOP}^{Asy} \approx \frac{\Omega_D\Omega_E}{\Gamma(\mu_D+1)\Gamma(\mu_E)}\sum_{n=0}^{\infty}\binom{\mu_D}{n}\frac{\theta^n}{(\theta-1)^{n-\mu_D}}\Gamma(\mu_E+n)(\bar{\gamma}_E\sqrt{\eta_E\alpha_{2_E}})^{\mu_E+n}$$
$$\times F_D^{(3)}(\mu_E+n;\frac{\mu_E}{2}-m_E,m_E,m_E;\mu_E;1-\eta_E,1-\sqrt{\eta_E\alpha_{2_E}}c_{1_E},1-\sqrt{\eta_E\alpha_{2_E}}c_{2_E}) \quad (30)$$

$$T_{\mathrm{SOP}^{Asy}} \leqslant \frac{\Gamma(\mu_E)(\mu_E)_N}{N!}\left(\frac{\theta\bar{\gamma}_E\sqrt{\eta_E\alpha_{2_E}}}{1-\theta}\right)^N{}_3F_1\left(-\mu_D,\mu_E+N,N+1,1;N+1;\frac{\theta\bar{\gamma}_E\sqrt{\eta_E\alpha_{2_E}}}{1-\theta}\right)$$
$$\times F_D^{(3)}(\mu_E+N;\frac{\mu_E}{2}-m_E,m_E,m_E;\mu_E;1-\eta_E,1-\sqrt{\eta_E\alpha_{2_E}}c_{1_E},1-\sqrt{\eta_E\alpha_{2_E}}c_{2_E}) \quad (31)$$

$$\mathrm{SOP}_{Asy}^{L} \approx \frac{\Omega_D\Omega_E\theta_D^{\mu}}{\Gamma(\mu_D+1)\Gamma(\mu_E)}\Gamma(\mu_D+\mu_E)(\bar{\gamma}_E\sqrt{\eta_E\alpha_{2_E}})^{\mu_D+\mu_E}$$
$$\times F_D^{(3)}(\mu_D+\mu_E;\frac{\mu_E}{2}-m_E,m_E,m_E;\mu_E;1-\eta_E,1-\sqrt{\eta_E\alpha_{2_E}}c_{1_E},1-\sqrt{\eta_E\alpha_{2_E}}c_{2_E}) \quad (32)$$

depends only on γ_E, another expression to evaluate I_3^{Asy} is also provided in (27), as shown at the top of this page. Next, inserting (25), (26), and (27) in (24) to yield $\bar{C}_s^{Asy}$ as shown in (28), as shown at the top of this page.

One can see that (28) is expressed in terms of $F_D^{(3)}(.)$ which denotes the Lauricella hypergeometric function of three variables as defined in [26, eq. (1.7.4)]. This function is not yet available as a built-in function in the popular software package such as MATLAB and MATHEMATICA. Thus, several works have used the Euler integral representation of $F_D^{(3)}(.)$ and a numerical method to calculate this function [28, Appendix V]. However, this methodology can be used

under a specific condition which is not satisfied in (28). Therefore, the efficient MATLAB code that is implemented in [29] to compute $F_D^{(3)}(.)$ even if Euler integral is not valid has been used in this paper.

Proof: See Appendix E. ■

Corollary 2: It can be noted that (28) included an infinite series. Therefore, a series convergence acceleration for a number of terms, N, that satisfies a certain figure of accuracy should be applied. This can be achieved by employing (29) that is provided on the top of the previous page. In (29), ${}_5F_2(.)$ stands for the hypergeometric function defined in [26, eq. (1.4.1), p. 42].

Proof: See Appendix F. ■

B. ASYMPTOTIC ANALYSIS OF SOP

Theorem 5: The asymptotic behaviour of SOP, SOP^{Asy}, over FB fading channel can be analysed by using (30) that is shown at the top of the previous page. It is worth mentioning that $\text{SOP}^{Asy} \approx \mathcal{G}_c \bar{\gamma}^{-\mathcal{G}_d}$ where $\mathcal{G}_c$ and $\mathcal{G}_d$ are the secrecy array gain and the secrecy diversity gain, respectively [30]. Hence, the secrecy diversity gain can be deduced from (30) to be $\mathcal{G}_d = \mu_D$ (please refer to Ω_D that is described after (2)).

Proof: See Appendix G. ■

Corollary 3: The infinite series of (30) can be truncated by N terms via using (31), as shown at the top of the previous page.

Proof: Utilizing the identity $\binom{a}{b} = \frac{\Gamma(a+1)}{b!\Gamma(a-b+1)}$ [26, eq. (1.1.17)] and following the same steps in Corollary 2, (31) is deduced and the proof is accomplished. ■

C. ASYMPTOTIC ANALYSIS OF SOP^L

The asymptotic expression of SOP^L, SOP^L_{Asy}, when $\bar{\gamma}_D \to \infty$ over FB fading scenario is derived in exact closed-form as given in (32), as shown at the top of the previous page. This expression is obtained via inserting $\theta\gamma_E$ instead of $\theta\gamma_E + \theta - 1$ in (74) and employing (59) and [26, eq. (1.i), p. 259].

VIII. PHYSICAL LAYER SECURITY OVER SPECIAL CASES OF FB FADING CHANNEL MODEL

It has been mentioned in [22], the FB fading channel is a versatile model for nearly most of the well known distributions. Accordingly, our derived secrecy performance metrics can be utilised for different scenarios of wireless communications channels that have not been yet done in the literature due to the complexity of their statistical characterization. For example, when $\kappa = K$, $\mu = 1$, $m \to \infty$, $\eta = q$, and $\varrho = r$ the Beckmann distribution is the result. Furthermore, the PDF and the CDF of $\kappa-\mu$ shadowed fading obtained from (2) or (5) and (4) or (6), respectively, after plugging $\kappa = K$, $\mu = \mu, m = m, \eta = 1$, and $\forall\varrho$. The ASC, the SOP, the SOP^L, and the SPSC for $\eta - \mu$ fading condition can be deduced by substituting $\kappa = 0$, $\mu = \mu$, $\eta = \eta$ and vanishing of both m and ϱ in our derived expressions.

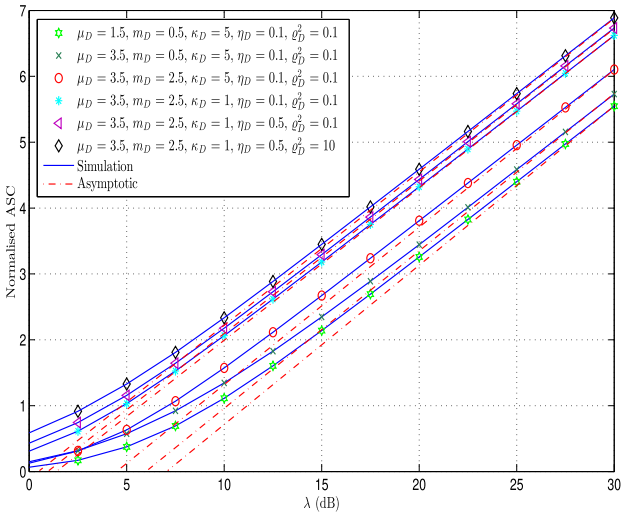

FIGURE 1. ASC versus λ for $\bar{\gamma}_E = 5$ dB, $\mu_E = 1.5$, $m_E = 1.5$, $\kappa_E = 1$, $\eta_E = 0.1$, $\varrho_E^2 = 0.1$.

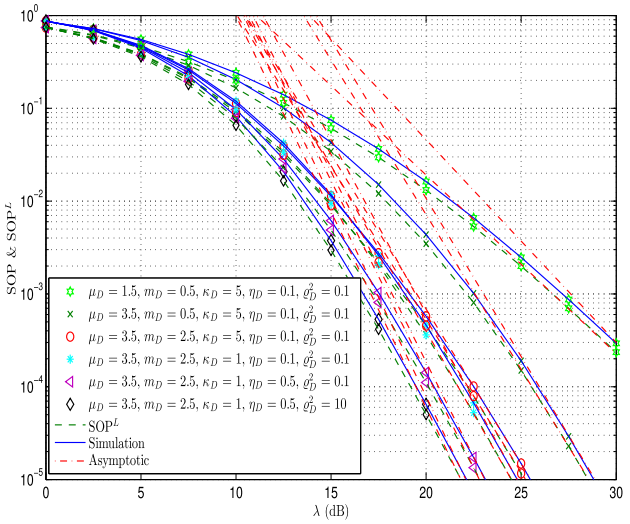

FIGURE 2. SOP and SOP^L versus λ for $\bar{\gamma}_E = 5$ dB, $\mu_E = 1.5$, $m_E = 1.5$, $\kappa_E = 1$, $\eta_E = 0.1$, $\varrho_E^2 = 0.1$, $R_s = 1$.

IX. NUMERICAL AND SIMULATION RESULTS

In this section, the numerical results of this work are verified via Monte Carlo simulations with 10^7 realizations. The parameters of main and wiretap channels are assumed to be independent and non-identically distributed random variables. In all figures, the markers represent the numerical results, whereas the solid and dashed lines explain their simulation and asymptotic counterparts. For the asymptotic results of (28) and (31), the number of terms, N, has been chosen to satisfy seven figure of accuracy.

Figs. 1, 2 and 3 illustrate the ASC, the SOP & SOP^L and the SPSC versus $\lambda = \bar{\gamma}_D/\bar{\gamma}_E$, respectively, for $\bar{\gamma}_E = 5$ dB, $\mu_E = 1.5$, $m_E = 1.5$, $\kappa_E = 1$, $\eta_E = 0.1$, $\varrho_E^2 = 0.1$ and different values of the fading parameters of Bob. From these figures, one can see that the secrecy performance improves

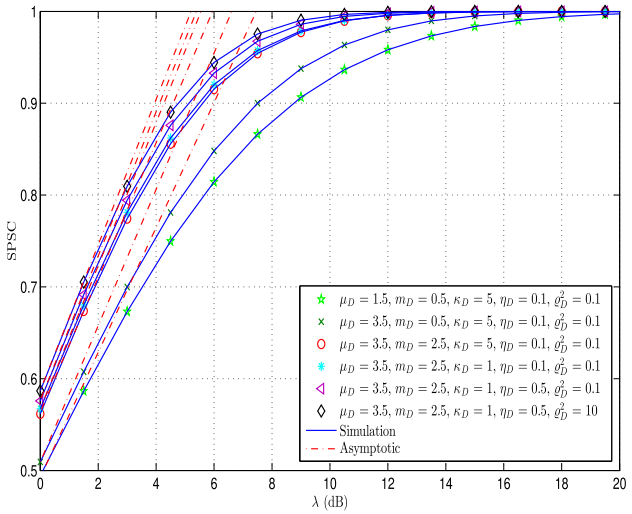

FIGURE 3. SPSC versus λ for $\bar{\gamma}_E = 5$ dB, $\mu_E = 1.5$, $m_E = 1.5$, $\kappa_E = 1$, $\eta_E = 0.1$, $\varrho_E^2 = 0.1$, $R_s = 1$.

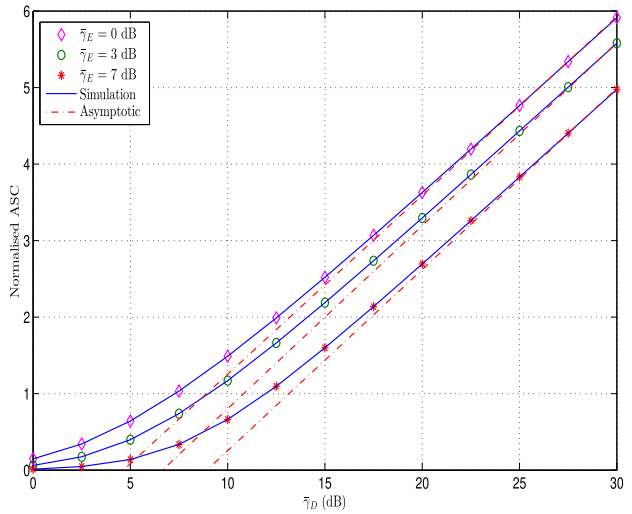

FIGURE 4. ASC versus $\bar{\gamma}_D$ for $\mu_D = \mu_E = 2.5$, $m_D = m_E = 1.5$, $\kappa_D = \kappa_E = 3$, $\eta_D = \eta_E = 0.5$, $\varrho_D^2 = \varrho_E^2 = 0.2$ and different values of $\bar{\gamma}_E$.

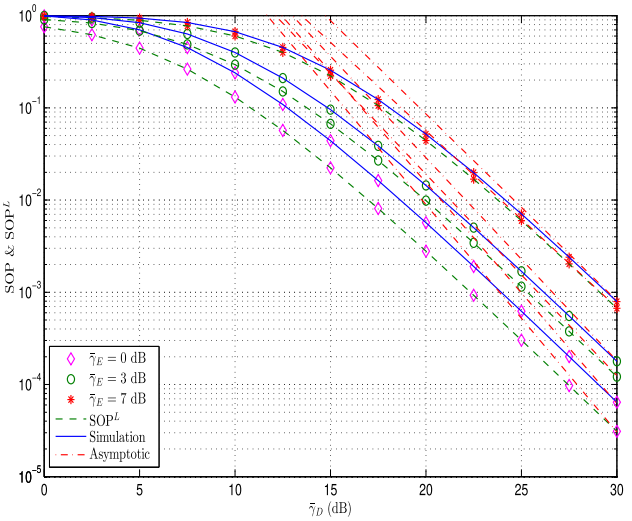

FIGURE 5. SOP & SOP^L versus $\bar{\gamma}_D$ for $\mu_D = \mu_E = 2.5$, $m_D = m_E = 1.5$, $\kappa_D = \kappa_E = 3$, $\eta_D = \eta_E = 0.5$, $\varrho_D^2 = \varrho_E^2 = 0.2$, $R_s = 1$ and different values of $\bar{\gamma}_E$.

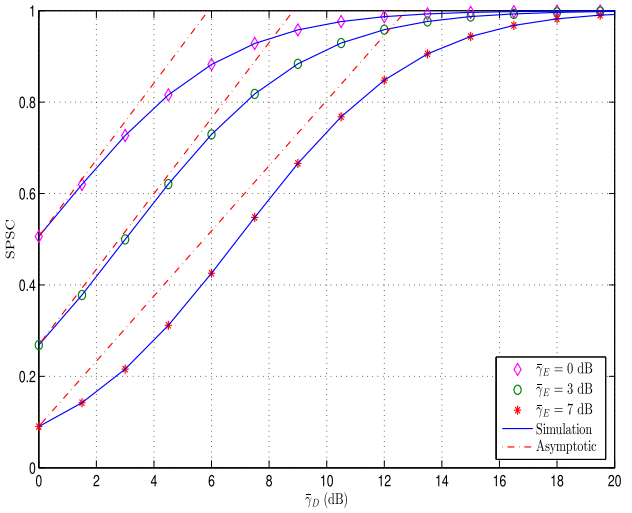

FIGURE 6. SPSC versus $\bar{\gamma}_D$ for $\mu_D = \mu_E = 2.5$, $m_D = m_E = 1.5$, $\kappa_D = \kappa_E = 3$, $\eta_D = \eta_E = 0.5$, $\varrho_D^2 = \varrho_E^2 = 0.2$, $R_s = 1$ and different values of $\bar{\gamma}_E$.

when μ_D, m_D, η_D, or/and ϱ_D^2 increase. This is because the increasing in μ_D or/and m_D correspond to a large number of the multipath clusters and the less shadowing impact at the Bob, respectively. Moreover, the improving in the values of η_D, or/and ϱ_D^2 mean a high power rate at the Bob, i.e., the total power of the in-phase components. on the contrary, the decreasing of κ_D increases the values of all the studied performance metrics. The main reason is the parameter κ_D represents the ratio between the total power of the dominant components and the total power of the scattered waves. For example, in Fig. 1, at $m_D = 0.5$, $\kappa_D = 5$, $\eta_D = 0.1$, $\varrho^2 = 0.1$ and $\lambda = 15$ dB (fixed), the ASC for $\mu_D = 3.5$ is nearly 10% higher than $\mu_D = 1.5$. In the same context, when $\mu_D = 3.5$ and m_D changes from 0.5 to 2.5, the ASC is increased by roughly 25%. Furthermore, the ASC for the scenario $\mu_D = 3.5$, $m_D = 2.5$, $\kappa_D = 1$, $\eta_D = 0.1$, and $\varrho_D^2 = 0.1$ at $\lambda = 15$ dB is approximately 2.139 whereas for $\eta_D = 0.5$ is 3.293 which is less than for $\varrho_D^2 = 10$ by nearly 5%. On the other side, the ASC for the previous scenario is decreased by roughly 16% when κ_D becomes 5. The impacts of the fading parameters on the provided results in Fig. 1 are confirmed by Figs. 2 and 3. In addition, from these figures, it is clear that the secrecy performance enhances when λ increases. This refers to the high $\bar{\gamma}_D$ in comparison with the $\bar{\gamma}_E$ which would lead to make the Alice-Bob channel better than the Alice-Eve channel. It is evident that the derived secrecy diversity gain, $\mathcal{G}_d = \mu_D$, is affirmed by Fig. 2 where the overall system performance improves with the increasing in μ_D and vice versa.

Figs. 4, 5, and 6 demonstrate the ASC, the SOP & SOP^L and the SPSC versus $\bar{\gamma}_D$, respectively, for $\mu_D = \mu_E = 2.5$, $m_D = m_E = 1.5$, $\kappa_D = \kappa_E = 3$, $\eta_D = \eta_E = 0.5$,

$\varrho_D^2 = \varrho_E^2 = 0.2$ and different values of $\bar{\gamma}_E$. As expected, a clear improvement can be noticed in the secrecy performance of the considered system when $\bar{\gamma}_E$ reduces. The reason is the large deterioration in the Alice-Eve wireless channel. For instance, in Fig. 4, at $\bar{\gamma}_D = 15$ dB (fixed), the ASC for $\bar{\gamma}_E = 7$ dB and $\bar{\gamma}_E = 3$ dB are approximately 1.598 and 2.189, respectively.

In all figures, the numerical results and the Monte Carlo simulations are in perfect match for any given scenario. Moreover, the asymptotic of the studied performance metrics becomes in a perfect match with the exact results when $\bar{\gamma}_D$ or λ increase which verify the correctness of our derived expressions. Another confirmation on the validation of the derived expressions is presented in Figs. 2 and 5 in which the SOP^L is less than or equal to the SOP.

X. CONCLUSION

This paper was dedicated to study the secrecy behaviour of the physical layer over Fluctuating Beckmann fading channel model. To be specific, the ASC, the SOP, the SOP^L, and the SPSC, were derived in novel exact expressions by using two cases for the values of the fading parameters. In the first case, the derived results were expressed in terms of EGBFHF. On the other side, the second case provided simple analytic exact mathematically tractable closed-form expressions via assuming μ and m for both Bob and Eve are even number and integer number, respectively. From the given results, a reduction in the values of the ASC, the SOP, the SOP^L, and the SPSC can be observed when the value of μ, m, η, or/and ϱ^2 of the Bob decrease. However, the secrecy performances of the system improves when κ of the Bob or/and γ_E reduce. To gain more insights on the overall system performance behaviour at high SNR of the Bob, the asymptotic expressions were derived. The results of this work can be employed to analyse the secrecy performance of the physical layer over a variety of fading channels with simple exact closed-form expressions.

APPENDIX A
PROOF OF THEOREM 1

Substituting (2) and (4) into (7), this yields

$$I_1 = \frac{\Omega_D \Omega_E}{\Gamma(\mu_D)\Gamma(\mu_E+1)} \int_0^\infty \ln(1+\gamma_D)\gamma_D^{\mu_D+\mu_E-1} \times \Phi_2^{(4)}\left(\frac{\mu_D}{2} - m_D, \frac{\mu_D}{2} - m_D, m_D, m_D; \mu_D; -\frac{\gamma_D}{\bar{\gamma}_D\sqrt{\eta_D\alpha_{2_D}}}, -\frac{\gamma_D\sqrt{\eta_D}}{\bar{\gamma}_D\sqrt{\alpha_{2_D}}}, -\frac{\gamma_D c_{1_D}}{\bar{\gamma}_D}, -\frac{\gamma_D c_{2_D}}{\bar{\gamma}_D}\right) \times \Phi_2^{(4)}\left(\frac{\mu_E}{2} - m_E, \frac{\mu_E}{2} - m_E, m_E, m_E; \mu_E+1; -\frac{\gamma_D}{\bar{\gamma}_E\sqrt{\eta_E\alpha_{2_E}}}, -\frac{\gamma_D\sqrt{\eta_E}}{\bar{\gamma}_E\sqrt{\alpha_{2_E}}}, -\frac{\gamma_D c_{1_E}}{\bar{\gamma}_E}, -\frac{\gamma_D c_{2_E}}{\bar{\gamma}_E}\right) d\gamma_D. \tag{33}$$

The exact closed-form solution of the integral in (33) is not available in the open literature. Therefore, to evaluate the above integral, we firstly express ln(.) in terms of the single variable Fox's H-function (FHF) by using the property [11, eq. (36)]

$$\ln(1+x) = H_{2,2}^{1,2}\left[x\middle|\begin{matrix}(1,1),(1,1)\\(1,1),(0,1)\end{matrix}\right] \tag{34}$$

For the confluent Lauricella hypergeometric function $\Phi_2^{(4)}(.)$, the following identity can be utilised [26, eq. (1.ii), pp. 259]

$$\Phi_2^{(4)}(a_1,a_2,a_3,a_4;b;-x_1\,t,-x_2\,t,-x_3\,t,-x_4\,t) = \frac{1}{t^{b-1}}\mathcal{L}^{-1}\left\{\frac{\Gamma(b)}{s^b}\left(1+\frac{x_1}{s}\right)^{-a_1}\left(1+\frac{x_2}{s}\right)^{-a_2} \times\left(1+\frac{x_3}{s}\right)^{-a_3}\left(1+\frac{x_4}{s}\right)^{-a_4}; s, t\right\}. \tag{35}$$

where $\Re(b) > 0$, $\Re(s) > 0$, $\{a_1, a_2, a_3, a_4\} \in \mathbb{R}$ and $\mathcal{L}^{-1}(.)$ is the inverse Laplace transform.

To compute the above inverse Laplace transform, the following identity is recalled [27, eq. (1.43)]

$$(1+x)^{-a} = \frac{1}{\Gamma(a)} H_{1,1}^{1,1}\left[x\middle|\begin{matrix}(1-a,1)\\(0,1)\end{matrix}\right]. \tag{36}$$

With the aid of (36) and using the form of Barnes-type contour integral of FHF [27, eq. (1.2) and [27, eq.(1.3)], the inverse Laplace transform of (35) can be rewritten as

$$\mathcal{L}^{-1}\left\{\frac{\Gamma(b)}{s^b}\left(1+\frac{x_1}{s}\right)^{-a_1}\left(1+\frac{x_2}{s}\right)^{-a_2}\left(1+\frac{x_3}{s}\right)^{-a_3} \times\left(1+\frac{x_4}{s}\right)^{-a_4}; s, t\right\} = \frac{\Gamma(b)}{t^{b-1}\Gamma(a_1)\Gamma(a_2)\Gamma(a_3)\Gamma(a_4)} \times\frac{1}{(2\pi j)^4}\int_{\mathcal{R}_1}\int_{\mathcal{R}_2}\int_{\mathcal{R}_3}\int_{\mathcal{R}_4}\Gamma(r_1)\Gamma(a_1-r_1)\Gamma(r_2)\Gamma(a_2-r_2) \times\Gamma(r_3)\Gamma(a_3-r_3)\Gamma(r_4)\Gamma(a_4-r_4)x_1^{-r_1}x_2^{-r_2}x_3^{-r_3}x_4^{-r_4} \times\mathcal{L}^{-1}\left\{s^{r_1+r_2+r_3+r_4-b}; s, t\right\}dr_1dr_2dr_3dr_4. \tag{37}$$

where $j = \sqrt{-1}$ and $\mathcal{R}_i$ for $i \in \{1,2,3,4\}$ represent the suitable closed contours from $\sigma_i - j\infty$ to $\sigma_i + j\infty$ and σ_i is a constant in the complex r_i-plane.

The inverse Laplace transform of (37) can be calculated as follows

$$\mathcal{L}^{-1}\left\{s^{r_1+r_2+r_3+r_4-b}; s, t\right\} = \frac{t^{b-r_1-r_2-r_3-r_4-1}}{\Gamma(b-r_1-r_2-r_3-r_4)}. \tag{38}$$

Substituting (38) into (37), yielding (39), as shown at the top of the next page.

Plugging (34) in (33) and employing (35) and (39) for both the confluent Lauricella hypergeometric functions $\Phi_2^{(4)}(.)$, one obtains (40), as shown at the top of the next page.

With the help of [31, eq. (4.293.10)], the inner integral, $\mathcal{K}_1$, of (43) can be be computed in exact closed-form as

$$\mathcal{K}_1 = \frac{\pi}{(\mu_D+\mu_E-\sum_{j=1}^8 r_j)\sin((\mu_D+\mu_E-\sum_{j=1}^8 r_j)\pi)}. \tag{41}$$

$$\mathcal{L}^{-1}\left\{\frac{\Gamma(b)}{s^b}\left(1+\frac{x_1}{s}\right)^{-a_1}\left(1+\frac{x_2}{s}\right)^{-a_2}\left(1+\frac{x_3}{s}\right)^{-a_3}\left(1+\frac{x_4}{s}\right)^{-a_4};s,t\right\}$$
$$=\frac{\Gamma(b)}{\Gamma(a_1)\Gamma(a_2)\Gamma(a_3)\Gamma(a_4)}t^{b-1}$$
$$\times\frac{1}{(2\pi j)^4}\int_{\mathcal{R}_1}\int_{\mathcal{R}_2}\int_{\mathcal{R}_3}\int_{\mathcal{R}_4}\frac{\Gamma(r_1)\Gamma(a_1-r_1)\Gamma(r_2)\Gamma(a_2-r_2)\Gamma(r_3)\Gamma(a_3-r_3)\Gamma(r_4)\Gamma(a_4-r_4)}{\Gamma(b-r_1-r_2-r_3-r_4)}$$
$$\times(xt)_1^{-r_1}(xt)_2^{-r_2}(xt)_3^{-r_3}(xt)_4^{-r_4}\,dr_1\,dr_2\,dr_3\,dr_4. \tag{39}$$

$$I_1=\frac{\Omega_D\Omega_E}{[\Gamma(\frac{\mu_D}{2}-m_D)\Gamma(\frac{\mu_E}{2}-m_E)\Gamma(m_D)\Gamma(m_E)]^2}$$
$$\times\frac{1}{(2\pi j)^8}\int_{\mathcal{R}_1}\cdots\int_{\mathcal{R}_8}\frac{[\prod_{j=1}^{8}\Gamma(r_j)][\prod_{j=1}^{2}\Gamma(\frac{\mu_D}{2}-m_D-r_j)\Gamma(m_D-r_{j+2})\Gamma(\frac{\mu_E}{2}-m_E-r_{j+4})\Gamma(m_E-r_{j+6})]}{\Gamma(\mu_D-r_1-\cdots-r_4)\Gamma(1+\mu_E-r_5-\cdots-r_8)}$$
$$\times\frac{1}{(\bar{\gamma}_D\sqrt{\eta_D\alpha_{2_D}})^{-r_1}}\left(\frac{\sqrt{\eta_D}}{\bar{\gamma}_D\sqrt{\alpha_{2_D}}}\right)^{-r_2}\left(\frac{c_{1_D}}{\bar{\gamma}_D}\right)^{-r_3}\left(\frac{c_{2_D}}{\bar{\gamma}_D}\right)^{-r_4}\frac{1}{(\bar{\gamma}_E\sqrt{\eta_E\alpha_{2_E}})^{-r_5}}\left(\frac{\sqrt{\eta_E}}{\bar{\gamma}_E\sqrt{\alpha_{2_E}}}\right)^{-r_6}\left(\frac{c_{1_E}}{\bar{\gamma}_E}\right)^{-r_7}\left(\frac{c_{2_E}}{\bar{\gamma}_E}\right)^{-r_8}$$
$$\times\underbrace{\int_0^\infty\gamma_D^{\mu_D+\mu_E-\sum_{j=1}^{8}r_j-1}\ln(1+\gamma_D)d\gamma_D}_{\mathcal{K}_1}\,dr_1\cdots dr_8. \tag{40}$$

Recalling the identities $a=\frac{\Gamma(1+a)}{\Gamma(a)}$ [31, eq. (8.331.1)] and $\sin(\pi a)=\frac{\pi}{a\Gamma(1-a)}$ [31, eq. (8.334.3)], (41) becomes

$$\mathcal{K}_1=\frac{[\Gamma(\mu_D+\mu_E-\sum_{j=1}^{8}r_j)]^2}{\Gamma(1+\mu_D+\mu_E-\sum_{j=1}^{8}r_j)}\times\Gamma(1-\mu_D-\mu_E+\sum_{j=1}^{8}r_j). \tag{42}$$

Inserting (42) in (40) with some algebraic manipulations, (43) is obtained as shown on the top of the next page.

It is worth noting that (43) can be written in exact expression in terms of the EGBFHF via using [27, eq. (A.1)] and this completes the proof of (10).

Following the same mathematical methodology of I_1, the proof for I_2 in (11) is accomplished. It can be observed (10) can be utilised to evaluate (11) by replacing each D and E by E and D, respectively.

For I_3, we substitute (2) into (9) to yield (44), as shown at the top of the next page. After that, by following the same steps of computing $\mathcal{K}_1$, $\mathcal{K}_2$ is expressed as

$$\mathcal{K}_2=\frac{[\Gamma(\mu_E-\sum_{j=1}^{4}r_j)]^2\Gamma(1-\mu_E+\sum_{j=1}^{4}r_j)}{\Gamma(1+\mu_E-\sum_{j=1}^{4}r_j)} \tag{45}$$

Plugging (45) in (44), we have (46), as shown at the top of the next page.

Making use of [27, eq. (A.1)], I_3 in (46) can be rewritten in exact expression as provided in (12) which completes the proof.

APPENDIX B
PROOF OF COROLLARY 1

For *Case_2*, I_1 can be calculated via inserting (5) and (6) in (7). Accordingly, this yields

$$I_1=\Omega_D\sum_{i_D=1}^{N_D(m_D,\mu_D)}\sum_{j_D=1}^{|\omega_{i_D}|}\frac{A_{i_Dj_D}}{(j_D-1)!}$$
$$\times\left[\int_0^\infty\gamma_D^{j_D-1}\ln(1+\gamma_D)e^{-\frac{\vartheta_{i_D}}{\bar{\gamma}_D}\gamma_D}d\gamma_D\right.$$
$$+\Omega_E\sum_{i_E=1}^{N_E(m_E,\mu_E)}\sum_{j_E=1}^{|\omega_{i_E}|}\frac{B_{i_Ej_E}}{(j_E-1)!}$$
$$\left.\int_0^\infty\gamma_D^{j_D+j_E-2}\ln(1+\gamma_D)e^{-\left(\frac{\vartheta_{i_D}}{\bar{\gamma}_D}+\frac{\vartheta_{i_E}}{\bar{\gamma}_E}\right)\gamma_D}d\gamma_D\right]. \tag{47}$$

With the aid of [32, eq. (47)], both integrals of (47) can be written in simple exact closed-form expressions as

$$\int_0^\infty x^{a-1}\ln(1+x)e^{-bx}dx=\Gamma(a)e^b\sum_{k=1}^{a}\frac{\Gamma(k-a,b)}{b^k}. \tag{48}$$

Using (48) and doing some algebraic simplifications, I_1 that is given in (13) is deduced and this completes the proof.

Replacing D and E by E and D, respectively, in (13), the result is I_2 for integer values of m_l and even numbers of μ_l as shown in (14).

Similarly, after plugging (5) in (9) and using (48), I_3 is expressed in exact closed-form as provided in (15) and the proof is accomplished.

$$I_1 = \frac{\Omega_D \Omega_E}{[\Gamma(\frac{\mu_D}{2} - m_D)\Gamma(\frac{\mu_E}{2} - m_E)\Gamma(m_D)\Gamma(m_E)]^2} \times \frac{1}{(2\pi j)^8} \int_{\mathcal{R}_1} \cdots \int_{\mathcal{R}_8} \frac{[\Gamma(\mu_D + \mu_E - \sum_{j=1}^{8} r_j)]^2 \Gamma(1 - \mu_D - \mu_E + \sum_{j=1}^{8} r_j)[\prod_{j=1}^{8} \Gamma(r_j)]}{\Gamma(1 + \mu_D + \mu_E - \sum_{j=1}^{8} r_j)} \times \frac{[\prod_{j=1}^{2} \Gamma(\frac{\mu_D}{2} - m_D - r_j)\Gamma(m_D - r_{j+2})\Gamma(\frac{\mu_E}{2} - m_E - r_{j+4})\Gamma(m_E - r_{j+6})]}{\Gamma(\mu_D - r_1 - \cdots - r_4)\Gamma(1 + \mu_E - r_5 - \cdots - r_8)} \frac{1}{(\bar{\gamma}_D \sqrt{\eta_D \alpha_{2_D}})^{-r_1}} \times \left(\frac{\sqrt{\eta_D}}{\bar{\gamma}_D \sqrt{\alpha_{2_D}}}\right)^{-r_2} \left(\frac{c_{1_D}}{\bar{\gamma}_D}\right)^{-r_3} \left(\frac{c_{2_D}}{\bar{\gamma}_D}\right)^{-r_4} \frac{1}{(\bar{\gamma}_E \sqrt{\eta_E \alpha_{2_E}})^{-r_5}} \left(\frac{\sqrt{\eta_E}}{\bar{\gamma}_E \sqrt{\alpha_{2_E}}}\right)^{-r_6} \left(\frac{c_{1_E}}{\bar{\gamma}_E}\right)^{-r_7} \left(\frac{c_{2_E}}{\bar{\gamma}_E}\right)^{-r_8} dr_1 \cdots dr_8. \quad (43)$$

$$I_3 = \frac{\Omega_E}{[\Gamma(\frac{\mu_E}{2} - m_E)\Gamma(m_E)]^2} \frac{1}{(2\pi j)^4} \int_{\mathcal{R}_1} \cdots \int_{\mathcal{R}_4} \frac{[\prod_{j=1}^{4} \Gamma(r_j)][\prod_{j=1}^{2} \Gamma(\frac{\mu_E}{2} - m_E - r_j)\Gamma(m_E - r_{j+2})]}{\Gamma(\mu_E - r_1 - \cdots - r_4)} \times \frac{1}{(\bar{\gamma}_E \sqrt{\eta_E \alpha_{2_E}})^{-r_1}} \left(\frac{\sqrt{\eta_E}}{\bar{\gamma}_E \sqrt{\alpha_{2_E}}}\right)^{-r_2} \left(\frac{c_{1_E}}{\bar{\gamma}_E}\right)^{-r_3} \left(\frac{c_{2_E}}{\bar{\gamma}_E}\right)^{-r_4} \underbrace{\int_0^{\infty} \gamma_E^{\mu_E - \sum_{j=1}^{4} r_j - 1} \ln(1 + \gamma_E) d\gamma_E}_{\mathcal{K}_2} dr_1 \cdots dr_4. \quad (44)$$

$$I_3 = \frac{\Omega_E}{[\Gamma(\frac{\mu_E}{2} - m_E)\Gamma(m_E)]^2} \frac{1}{(2\pi j)^4} \int_{\mathcal{R}_1} \cdots \int_{\mathcal{R}_4} \frac{\Gamma(1 - \mu_E + \sum_{j=1}^{4} r_j)[\Gamma(\mu_E - \sum_{j=1}^{4} r_j)]^2}{\Gamma(1 + \mu_E - \sum_{j=1}^{4} r_j)[\prod_{j=1}^{4} \Gamma(r_j)]} \times \frac{[\prod_{j=1}^{2} \Gamma(\frac{\mu_E}{2} - m_E - r_j)\Gamma(m_E - r_{j+2})]}{\Gamma(\mu_E - \sum_{j=1}^{4} r_j)} \frac{1}{(\bar{\gamma}_E \sqrt{\eta_E \alpha_{2_E}})^{-r_1}} \left(\frac{\sqrt{\eta_E}}{\bar{\gamma}_E \sqrt{\alpha_{2_E}}}\right)^{-r_2} \left(\frac{c_{1_E}}{\bar{\gamma}_E}\right)^{-r_3} \left(\frac{c_{2_E}}{\bar{\gamma}_E}\right)^{-r_4} dr_1 \cdots dr_4. \quad (46)$$

$$\text{SOP} = \frac{\Omega_D \Omega_E}{[\Gamma(\frac{\mu_D}{2} - m_D)\Gamma(\frac{\mu_E}{2} - m_E)\Gamma(m_D)\Gamma(m_E)]^2} \times \frac{1}{(2\pi j)^8} \int_{\mathcal{R}_1} \cdots \int_{\mathcal{R}_8} \frac{[\prod_{j=1}^{8} \Gamma(r_j)][\prod_{j=1}^{2} \Gamma(\frac{\mu_E}{2} - m_E - r_j)\Gamma(m_E - r_{j+2})\Gamma(\frac{\mu_D}{2} - m_D - r_{j+4})\Gamma(m_D - r_{j+6})]}{\Gamma(1 + \mu_E - r_1 - \cdots - r_4)\Gamma(\mu_D - r_5 - \cdots - r_8)} \times \frac{1}{(\bar{\gamma}_E \sqrt{\eta_E \alpha_{2_E}})^{-r_1}} \left(\frac{\sqrt{\eta_E}}{\bar{\gamma}_E \sqrt{\alpha_{2_E}}}\right)^{-r_2} \left(\frac{c_{1_E}}{\bar{\gamma}_E}\right)^{-r_3} \left(\frac{c_{2_E}}{\bar{\gamma}_E}\right)^{-r_4} \frac{1}{(\bar{\gamma}_D \sqrt{\eta_D \alpha_{2_D}})^{-r_5}} \left(\frac{\sqrt{\eta_D}}{\bar{\gamma}_D \sqrt{\alpha_{2_D}}}\right)^{-r_6} \left(\frac{c_{1_D}}{\bar{\gamma}_D}\right)^{-r_7} \left(\frac{c_{2_D}}{\bar{\gamma}_D}\right)^{-r_8} \times \underbrace{\int_0^{\infty} \gamma_E^{\mu_E - \sum_{j=1}^{4} r_j - 1} (\theta\gamma_E + \theta - 1)^{\mu_D - \sum_{j=5}^{8} r_j} d\gamma_E}_{\mathcal{K}_3} dr_1 \cdots dr_8. \quad (50)$$

APPENDIX C
PROOF OF THEOREM 2

Inserting (2) and (4) in (17), the result is

$$\text{SOP} = \frac{\Omega_D \Omega_E}{\Gamma(\mu_E)\Gamma(\mu_D + 1)} \int_0^{\infty} (\theta\gamma_E + \theta - 1)^{\mu_D} \gamma_E^{\mu_E - 1} \times \Phi_2^{(4)}\left(\frac{\mu_E}{2} - m_E, \frac{\mu_E}{2} - m_E, m_E, m_E; \mu_E; -\frac{\gamma_E}{\bar{\gamma}_E \sqrt{\eta_E \alpha_{2_E}}}, -\frac{\gamma_E \sqrt{\eta_E}}{\bar{\gamma}_E \sqrt{\alpha_{2_E}}}, -\frac{\gamma_E c_{1_E}}{\bar{\gamma}_E}, -\frac{\gamma_E c_{2_E}}{\bar{\gamma}_E}\right) \times \Phi_2^{(4)}\left(\frac{\mu_D}{2} - m_D, \frac{\mu_D}{2} - m_D, m_D, m_D; \mu_D + 1; -\frac{(\theta\gamma_E + \theta - 1)}{\bar{\gamma}_D \sqrt{\eta_D \alpha_{2_D}}}, -\frac{(\theta\gamma_E + \theta - 1)\sqrt{\eta_D}}{\bar{\gamma}_D \sqrt{\alpha_{2_D}}}, -\frac{(\theta\gamma_E + \theta - 1)c_{1_D}}{\bar{\gamma}_D}, -\frac{(\theta\gamma_E + \theta - 1)c_{2_D}}{\bar{\gamma}_D}\right) d\gamma_E. \quad (49)$$

To solve the integral in (49), we recall (35) and (39) for both the confluent Lauricella hypergeometric functions $\Phi_2^{(4)}(.)$. Hence, we have (50), as shown at the top of this page.

Performing some mathematical manipulations and utilising [31, eq. (3.194.3)], $\mathcal{K}_3$ of (50) can be evaluated in exact closed-form as follows

$$\mathcal{K}_3 = \theta^{-\mu_E + \sum_{j=1}^{4} r_j} (\theta - 1)^{\mu_D + \mu_E - \sum_{j=1}^{8} r_j} \times B(\mu_E - \sum_{j=1}^{4} r_j, -\mu_D - \mu_E + \sum_{j=1}^{8} r_j). \quad (51)$$

where $B(.,.)$ is the Beta function defined in [26, eq. (1.1.43)].

$$\begin{aligned}\text{SOP} = {} & \frac{\Omega_D\Omega_E}{[\Gamma(\frac{\mu_D}{2}-m_D)\Gamma(\frac{\mu_E}{2}-m_E)\Gamma(m_D)\Gamma(m_E)]^2}\frac{(\theta-1)^{\mu_D+\mu_E}}{\theta^{\mu_E}} \\ & \times\frac{1}{(2\pi j)^8}\int_{\mathcal{R}_1}\cdots\int_{\mathcal{R}_8}\frac{[\prod_{j=1}^{8}\Gamma(r_j)][\prod_{j=1}^{2}\Gamma(\frac{\mu_E}{2}-m_E-r_j)\Gamma(m_E-r_{j+2})\Gamma(\frac{\mu_D}{2}-m_D-r_{j+4})\Gamma(m_D-r_{j+6})]}{\Gamma(1+\mu_E-r_1-\cdots-r_4)\Gamma(\mu_D-r_5-\cdots-r_8)} \\ & \times\frac{\Gamma(\mu_E-\sum_{j=1}^{4}r_j)\Gamma(-\mu_D-\mu_E+\sum_{j=1}^{8}r_j)}{\Gamma(-\mu_D+\sum_{j=5}^{8}r_j)}\left(\frac{(\theta-1)}{\theta\bar{\gamma}_E\sqrt{\eta_E\alpha_{2_E}}}\right)^{-r_1}\left(\frac{(\theta-1)\sqrt{\eta_E}}{\theta\bar{\gamma}_E\sqrt{\alpha_{2_E}}}\right)^{-r_2}\left(\frac{(\theta-1)c_{1_E}}{\theta\bar{\gamma}_E}\right)^{-r_3} \\ & \times\left(\frac{(\theta-1)c_{2_E}}{\theta\bar{\gamma}_E}\right)^{-r_4}\left(\frac{(\theta-1)}{\bar{\gamma}_D\sqrt{\eta_D\alpha_{2_D}}}\right)^{-r_5}\left(\frac{(\theta-1)\sqrt{\eta_D}}{\bar{\gamma}_D\sqrt{\alpha_{2_D}}}\right)^{-r_6}\left(\frac{(\theta-1)c_{1_D}}{\bar{\gamma}_D}\right)^{-r_7}\left(\frac{(\theta-1)c_{2_D}}{\bar{\gamma}_D}\right)^{-r_8}dr_1\cdots dr_8. \end{aligned} \tag{53}$$

Invoking the identity $B(x,y)=\frac{\Gamma(x)\Gamma(y)}{\Gamma(x+y)}$ [26, eq. (1.1.47)], (51) can be rewritten as

$$\begin{aligned}\mathcal{K}_3 = {} & \frac{\Gamma(\mu_E-\sum_{j=1}^{4}r_j)\Gamma(-\mu_D-\mu_E+\sum_{j=1}^{8}r_j)}{\Gamma(-\mu_D+\sum_{j=5}^{8}r_j)} \\ & \times\theta^{-\mu_E+\sum_{j=1}^{4}r_j}(\theta-1)^{\mu_D+\mu_E-\sum_{j=1}^{8}r_j}. \end{aligned} \tag{52}$$

Plugging (52) in (50) to yield (53) that is shown at the top of this page.

Next, recognising the definition of the EGBFHF [27, eq. (A.1)] for (53), the proof of SOP in (18) is achieved.

The SOP for *Case_2* can be calculated by substituting (5) and (6) in (17) and using the fact $\int_0^\infty f_\gamma(\gamma)d\gamma \triangleq 1$. Hence, we have

$$\begin{aligned}\text{SOP} = {} & 1+\Omega_D\Omega_E\sum_{i_E=1}^{N_E(m_E,\mu_E)}\sum_{j_E=1}^{|\omega_{i_E}|}\frac{A_{i_Ej_E}}{(j_E-1)!} \\ & \times\sum_{i_D=1}^{N_D(m_D,\mu_D)}\sum_{j_D=1}^{|\omega_{i_D}|}\frac{B_{i_Dj_D}}{(j_D-1)!} \\ & \times\underbrace{\int_0^\infty\gamma_E^{j_E-1}(\theta\gamma_E+\theta-1)^{j_D-1}e^{-\frac{\vartheta_{i_E}}{\bar{\gamma}_E}\gamma_E-\frac{(\theta\gamma_E+\theta-1)\vartheta_{i_D}}{\bar{\gamma}_D}}d\gamma_E}_{\mathcal{K}_4} \end{aligned} \tag{54}$$

Carrying out some mathematical manipulations on $\mathcal{K}_4$ of (54) to yield

$$\begin{aligned}\mathcal{K}_4 = {} & (\theta-1)^{j_D-1}e^{-(\theta-1)\frac{\vartheta_{i_D}}{\bar{\gamma}_D}} \\ & \times\int_0^\infty\gamma_E^{j_E-1}\left(1+\frac{\theta}{\theta-1}\gamma_E\right)^{j_D-1}e^{-\left(\frac{\vartheta_{i_E}}{\bar{\gamma}_E}+\frac{\theta\vartheta_{i_D}}{\bar{\gamma}_D}\right)\gamma_E}d\gamma_E. \end{aligned} \tag{55}$$

Applying the identity $(1+a)^b=\sum_{k=0}^{b}\binom{b}{k}a^k$ [31, eq. (1.111)] for (55), we obtain

$$\begin{aligned}\mathcal{K}_4 = {} & (\theta-1)^{j_D-1}e^{-(\theta-1)\frac{\vartheta_{i_D}}{\bar{\gamma}_D}}\sum_{r=0}^{j_D-1}\binom{j_D-1}{r}\left(\frac{\theta}{\theta-1}\right)^r \\ & \times\int_0^\infty\gamma_E^{j_E+r-1}e^{-\left(\frac{\vartheta_{i_E}}{\bar{\gamma}_E}+\frac{\theta\vartheta_{i_D}}{\bar{\gamma}_D}\right)\gamma_E}d\gamma_E. \end{aligned} \tag{56}$$

With the aid of [31, eq. (3.381.4)], the integral in (56) can be evaluated as

$$\begin{aligned}\mathcal{K}_4 = {} & (\theta-1)^{j_D-1}e^{-(\theta-1)\frac{\vartheta_{i_D}}{\bar{\gamma}_D}}\sum_{r=0}^{j_D-1}\binom{j_D-1}{r} \\ & \times\left(\frac{\theta}{\theta-1}\right)^r\frac{\Gamma(j_E+r)}{(\frac{\vartheta_{i_E}}{\bar{\gamma}_E}+\frac{\theta\vartheta_{i_D}}{\bar{\gamma}_D})^{j_E+r}}. \end{aligned} \tag{57}$$

Plugging (57) in (54) and performing some mathematical operations, the result is (19) and the proof is completed.

APPENDIX D
PROOF OF THEOREM 3

Substituting (2) and (4) in (20), this yields

$$\begin{aligned}\text{SOP}^L = {} & \frac{\Omega_D\Omega_E}{\Gamma(\mu_E)\Gamma(\mu_D+1)}\theta^{\mu_D}\int_0^\infty\gamma_E^{\mu_E+\mu_D-1} \\ & \times\Phi_2^{(4)}\left(\frac{\mu_E}{2}-m_E,\frac{\mu_E}{2}-m_E,m_E,m_E;\mu_E;\right. \\ & \left.-\frac{\gamma_E}{\bar{\gamma}_E\sqrt{\eta_E\alpha_{2_E}}},-\frac{\sqrt{\eta_E}}{\bar{\gamma}_E\sqrt{\alpha_{2_E}}}\gamma_E,-\frac{c_{1_E}}{\bar{\gamma}_E}\gamma_E,-\frac{c_{2_E}}{\bar{\gamma}_E}\gamma_E\right) \\ & \times\Phi_2^{(4)}\left(\frac{\mu_D}{2}-m_D,\frac{\mu_D}{2}-m_D,m_D,m_D;\mu_D+1;\right. \\ & -\frac{\theta}{\bar{\gamma}_D\sqrt{\eta_D\alpha_{2_D}}}\gamma_E,-\frac{\theta\sqrt{\eta_D}}{\bar{\gamma}_D\sqrt{\alpha_{2_D}}}\gamma_E, \\ & \left.-\frac{\theta c_{1_D}}{\bar{\gamma}_D}\gamma_E,-\frac{\theta c_{2_D}}{\bar{\gamma}_D}\gamma_E\right)d\gamma_E. \end{aligned} \tag{58}$$

To calculate the integral in (58), the following property is used [33, p. 177]

$$\begin{aligned} & e^{-c_i}\Phi_2^{(n)}(a_1,\cdots,a_n;b;c_1,\cdots,c_n) \\ & =\Phi_2^{(n)}(a_1,.,a_{i-1},b-a_1-.-a_n,a_{i+1},.,a_n;b; \\ & \quad c_1-c_i,\cdots,c_{i-1}-c_i,-c_i,c_{i+1}-c_i,\cdots,c_n-c_i). \end{aligned} \tag{59}$$

Accordingly, both the confluent Lauricella hypergeometric functions $\Phi_2^{(4)}(.)$ of (59) become

$$\begin{aligned} & \Phi_2^{(4)}\left(\frac{\mu_E}{2}-m_E,\frac{\mu_E}{2}-m_E,m_E,m_E;\mu_E;\right. \\ & \quad\left.-\frac{\gamma_E}{\bar{\gamma}_E\sqrt{\eta_E\alpha_{2_E}}},-\frac{\sqrt{\eta_E}}{\bar{\gamma}_E\sqrt{\alpha_{2_E}}}\gamma_E,-\frac{c_{1_E}}{\bar{\gamma}_E}\gamma_E,-\frac{c_{2_E}}{\bar{\gamma}_E}\gamma_E\right) \end{aligned}$$

$$\mathrm{SOP}^{L} = \frac{\Omega_D \Omega_E}{\Gamma(\frac{\mu_D}{2} - m_D)\Gamma(\frac{\mu_E}{2} - m_E)[\Gamma(m_D)\Gamma(m_E)]^2}\theta^{\mu} \times \frac{1}{(2\pi j)^6}\int_{\mathcal{R}_1}\cdots\int_{\mathcal{R}_6} \frac{[\prod_{j=1}^{6}\Gamma(r_j)]\Gamma(\frac{\mu_E}{2} - m_E - r_1)\Gamma(\frac{\mu_D}{2} - m_D - r_4)[\prod_{j=2}^{3}\Gamma(m_E - r_j)\Gamma(m_D - r_{j+3})]}{\Gamma(\mu_E - r_1 - \cdots - r_3)\Gamma(1 + \mu_D - r_4 - \cdots - r_6)} \times \left(\frac{\eta_E - 1}{\bar{\gamma}_E\sqrt{\eta_E\alpha_{2_E}}}\right)^{-r_1}\left(\frac{\sqrt{\eta_E\alpha_{2_E}}c_{1_E} - 1}{\bar{\gamma}_E\sqrt{\eta_E\alpha_{2_E}}}\right)^{-r_2}\left(\frac{\sqrt{\eta_E\alpha_{2_E}}c_{2_E} - 1}{\bar{\gamma}_E\sqrt{\eta_E\alpha_{2_E}}}\right)^{-r_3}\left(\frac{(\eta_D - 1)\theta}{\bar{\gamma}_D\sqrt{\eta_D\alpha_{2_D}}}\right)^{-r_4}\left(\frac{(\sqrt{\eta_D\alpha_{2_D}}c_{1_D} - 1)\theta}{\bar{\gamma}_D\sqrt{\eta_D\alpha_{2_D}}}\right)^{-r_5} \times \left(\frac{(\sqrt{\eta_D\alpha_{2_D}}c_{2_D} - 1)\theta}{\bar{\gamma}_D\sqrt{\eta_D\alpha_{2_D}}}\right)^{-r_6} \underbrace{\int_0^{\infty}\gamma_E^{\mu_D+\mu_E-\sum_{j=1}^{6}r_j-1}e^{-\left(\frac{1}{\bar{\gamma}_E\sqrt{\eta_E\alpha_{2_E}}}+\frac{\theta}{\bar{\gamma}_D\sqrt{\eta_D\alpha_{2_D}}}\right)\gamma_E}d\gamma_E}_{\mathcal{K}_5} dr_1\cdots dr_6. \quad (63)$$

$$= e^{-\frac{\gamma_E}{\bar{\gamma}_E\sqrt{\eta_E\alpha_{2_E}}}}\Phi_2^{(4)}\Bigg(0, \frac{\mu_E}{2} - m_E, m_E, m_E; \mu_E; \frac{\gamma_E}{\bar{\gamma}_E\sqrt{\eta_E\alpha_{2_E}}}, \frac{1-\eta_E}{\bar{\gamma}_E\sqrt{\eta_E\alpha_{2_E}}}\gamma_E, \frac{1-\sqrt{\eta_E\alpha_{2_E}}c_{1_E}}{\bar{\gamma}_E\sqrt{\eta_E\alpha_{2_E}}}\gamma_E, \frac{1-\sqrt{\eta_E\alpha_{2_E}}c_{2_E}}{\bar{\gamma}_E\sqrt{\eta_E\alpha_{2_E}}}\gamma_E\Bigg). \quad (60)$$

and

$$\Phi_2^{(4)}\Bigg(\frac{\mu_D}{2} - m_D, \frac{\mu_D}{2} - m_D, m_D, m_D; \mu_D + 1; -\frac{\theta}{\bar{\gamma}_D\sqrt{\eta_D\alpha_{2_D}}}\gamma_E, -\frac{\theta\sqrt{\eta_D}}{\bar{\gamma}_D\sqrt{\alpha_{2_D}}}\gamma_E, -\frac{\theta c_{1_D}}{\bar{\gamma}_D}\gamma_E, -\frac{\theta c_{2_D}}{\bar{\gamma}_D}\gamma_E\Bigg)$$
$$= e^{-\frac{\theta}{\bar{\gamma}_D\sqrt{\eta_D\alpha_{2_D}}}\gamma_E}\Phi_2^{(4)}\Bigg(0, \frac{\mu_D}{2} - m_D, m_D, m_D; \mu_D + 1; \frac{\theta}{\bar{\gamma}_D\sqrt{\eta_D\alpha_{2_D}}}\gamma_E, \frac{(1-\eta_D)\theta}{\bar{\gamma}_D\sqrt{\eta_D\alpha_{2_D}}}\gamma_E, \frac{(1-\sqrt{\eta_D\alpha_{2_D}}c_{1_D})\theta}{\bar{\gamma}_D\sqrt{\eta_D\alpha_{2_D}}}\gamma_E, \frac{(1-\sqrt{\eta_D\alpha_{2_D}}c_{2_D})\theta}{\bar{\gamma}_D\sqrt{\eta_D\alpha_{2_D}}}\gamma_E\Bigg). \quad (61)$$

Inserting (60) and (61) in (58), we have

$$\mathrm{SOP}^{L} = \frac{\Omega_D\Omega_E}{\Gamma(\mu_E)\Gamma(\mu_D+1)}\theta^{\mu_D}\int_0^{\infty}\gamma_E^{\mu_E+\mu_D-1} \times e^{-\left(\frac{1}{\bar{\gamma}_E\sqrt{\eta_E\alpha_{2_E}}}+\frac{\theta}{\bar{\gamma}_D\sqrt{\eta_D\alpha_{2_D}}}\right)\gamma_E} \times\Phi_2^{(4)}\Bigg(0, \frac{\mu_E}{2} - m_E, m_E, m_E; \mu_E; \frac{\gamma_E}{\bar{\gamma}_E\sqrt{\eta_E\alpha_{2_E}}}, \frac{1-\eta_E}{\bar{\gamma}_E\sqrt{\eta_E\alpha_{2_E}}}\gamma_E, \frac{1-\sqrt{\eta_E\alpha_{2_E}}c_{1_E}}{\bar{\gamma}_E\sqrt{\eta_E\alpha_{2_E}}}\gamma_E, \frac{1-\sqrt{\eta_E\alpha_{2_E}}c_{2_E}}{\bar{\gamma}_E\sqrt{\eta_E\alpha_{2_E}}}\gamma_E\Bigg) \times\Phi_2^{(4)}\Bigg(0, \frac{\mu_D}{2} - m_D, m_D, m_D; \mu_D + 1; \frac{\theta}{\bar{\gamma}_D\sqrt{\eta_D\alpha_{2_D}}}\gamma_E, \frac{(1-\eta_D)\theta}{\bar{\gamma}_D\sqrt{\eta_D\alpha_{2_D}}}\gamma_E, \frac{(1-\sqrt{\eta_D\alpha_{2_D}}c_{1_D})\theta}{\bar{\gamma}_D\sqrt{\eta_D\alpha_{2_D}}}\gamma_E, \frac{(1-\sqrt{\eta_D\alpha_{2_D}}c_{2_D})\theta}{\bar{\gamma}_D\sqrt{\eta_D\alpha_{2_D}}}\gamma_E\Bigg)d\gamma_E. \quad (62)$$

Recalling (35) and (39) for both $\Phi_2^{(4)}(.)$ of (62) to yield (63), as shown at the top of this page.

With the aid of [31, eq. (3.381.4)], $\mathcal{K}_5$ of (63) becomes

$$\mathcal{K}_5 = \frac{\Gamma\left(\mu_D + \mu_E - \sum_{j=1}^{6} r_j\right)}{\phi^{\mu_D+\mu_E-\sum_{j=1}^{6}r_j}}. \quad (64)$$

where $\phi = \frac{1}{\bar{\gamma}_E\sqrt{\eta_E\alpha_{2_E}}} + \frac{\theta}{\bar{\gamma}_D\sqrt{\eta_D\alpha_{2_D}}}$.

Plugging (64) in (63) and doing some algebraic operations, (65) is yielded as shown at the top of the next page.

With the help of [27, eq. (A.1)], the SOP^{L} of (65) is expressed in exact mathematically tractable format as given in (21) and this completes the proof.

For *Case_2*, SOP^{L} can be evaluated by plugging (5) and (6) in (20) and utilising $\int_0^{\infty} f_{\gamma}(\gamma)d\gamma \triangleq 1$. Thus, this yields

$$\mathrm{SOP}^{L} = 1 + \Omega_D\Omega_E\sum_{i_E=1}^{N_E(m_E,\mu_E)}\sum_{j_E=1}^{|\omega_{i_E}|}\frac{A_{i_Ej_E}}{(j_E-1)!} \times \sum_{i_D=1}^{N_D(m_D,\mu_D)}\sum_{j_D=1}^{|\omega_{i_D}|}\frac{B_{i_Dj_D}}{(j_D-1)!}\theta^{j_D-1} \times \underbrace{\int_0^{\infty}\gamma_E^{j_D+j_E-2}e^{-\left(\frac{\vartheta_{i_E}}{\bar{\gamma}_E}+\frac{\theta\vartheta_{i_D}}{\bar{\gamma}_D}\right)\gamma_E}d\gamma_E}_{\mathcal{K}_6}. \quad (66)$$

The above integral, $\mathcal{K}_6$, can be computed by using [31, eq. (3.381.4)] as follows

$$\mathcal{K}_6 = \frac{\Gamma(j_D+j_E-1)}{\left(\frac{\vartheta_{i_E}}{\bar{\gamma}_E}+\frac{\theta\vartheta_{i_D}}{\bar{\gamma}_D}\right)^{j_D+j_E-1}}. \quad (67)$$

Next, substituting (67) into (66) to obtain (22) and this completes the proof.

APPENDIX E
PROOF OF THEOREM 4

When $\bar{\gamma}_D \to \infty$, the fact that $\Phi_2^{(4)}(\frac{\mu_D}{2} - m_D, \frac{\mu_D}{2} - m_D, m_D, m_D; \mu_D; 0, 0, 0, 0) = 1$ [28] can be used in (33). Accordingly, we have

$$I_1^{Asy} = \frac{\Omega_D\Omega_E}{\Gamma(\mu_D)\Gamma(\mu_E+1)}\int_0^{\infty}\ln(1+\gamma_D)\gamma_D^{\mu_D+\mu_E-1}$$

$$\mathrm{SOP}^{L} = \frac{\Omega_D \Omega_E \theta^{\mu}}{\phi^{\mu_D+\mu_E}\Gamma(\frac{\mu_D}{2}-m_D)\Gamma(\frac{\mu_E}{2}-m_E)[\Gamma(m_D)\Gamma(m_E)]^2} \times \frac{1}{(2\pi j)^6}\int_{\mathcal{R}_1}\cdots\int_{\mathcal{R}_6}\frac{\Gamma\left(\mu_D+\mu_E-\sum_{j=1}^{6}r_j\right)[\prod_{j=1}^{6}\Gamma(r_j)]\Gamma(\frac{\mu_E}{2}-m_E-r_1)\Gamma(\frac{\mu_D}{2}-m_D-r_4)}{\Gamma(\mu_E-r_1-\cdots-r_3)} \times \frac{[\prod_{j=2}^{3}\Gamma(m_E-r_j)\Gamma(m_D-r_{j+3})]}{\Gamma(1+\mu_D-r_4-\cdots-r_6)}\left(\frac{\eta_E-1}{\phi\bar{\gamma}_E\sqrt{\eta_E\alpha_{2_E}}}\right)^{-r_1}\left(\frac{\sqrt{\eta_E\alpha_{2_E}}c_{1_E}-1}{\phi\bar{\gamma}_E\sqrt{\eta_E\alpha_{2_E}}}\right)^{-r_2}\left(\frac{\sqrt{\eta_E\alpha_{2_E}}c_{2_E}-1}{\phi\bar{\gamma}_E\sqrt{\eta_E\alpha_{2_E}}}\right)^{-r_3} \times\left(\frac{(\eta_D-1)\theta}{\phi\bar{\gamma}_D\sqrt{\eta_D\alpha_{2_D}}}\right)^{-r_4}\left(\frac{(\sqrt{\eta_D\alpha_{2_D}}c_{1_D}-1)\theta}{\phi\bar{\gamma}_D\sqrt{\eta_D\alpha_{2_D}}}\right)^{-r_5}\left(\frac{(\sqrt{\eta_D\alpha_{2_D}}c_{2_D}-1)\theta}{\phi\bar{\gamma}_D\sqrt{\eta_D\alpha_{2_D}}}\right)^{-r_6}dr_1\cdots dr_6. \quad (65)$$

$$\times\Phi_2^{(4)}\left(\frac{\mu_E}{2}-m_E,\frac{\mu_E}{2}-m_E,m_E,m_E;\mu_E+1; -\frac{\gamma_D}{\bar{\gamma}_E\sqrt{\eta_E\alpha_{2_E}}},-\frac{\sqrt{\eta_E}\gamma_D}{\bar{\gamma}_E\sqrt{\alpha_{2_E}}},-\frac{c_{1_E}\gamma_D}{\bar{\gamma}_E},-\frac{c_{2_E}\gamma_D}{\bar{\gamma}_E}\right)d\gamma_D. \quad (68)$$

To solve the integral of (68), the following identity can be employed [26, eq. (1.2.23), p. 34]

$$\ln(1+x) = x\,{}_2F_1(1,1;2;,-x) \quad (69)$$

where ${}_2F_1(.)$ is another format of the hypergeometric function defined in [26, eq. (1.2.2), p. 29].

Using [26, eq. (1.2.2), p. 29] for (69) and inserting the result along with (59) in (68) to yield

$$I_1^{Asy} = \frac{\Omega_D\Omega_E}{\Gamma(\mu_D)\Gamma(\mu_E+1)}\sum_{n=0}^{\infty}\frac{(1)_n(1)_n}{(2)_n n!}(-1)^n \times\int_0^{\infty}\gamma_D^{\mu_D+\mu_E+n}e^{-\frac{\gamma_D}{\bar{\gamma}_E\sqrt{\eta_E\alpha_{2_E}}}} \times\Phi_2^{(3)}\left(\frac{\mu_E}{2}-m_E,m_E,m_E;\mu_E+1;\frac{(1-\eta_E)\gamma_D}{\bar{\gamma}_E\sqrt{\eta_E\alpha_{2_E}}}, \frac{(1-\sqrt{\eta_E\alpha_{2_E}}c_{1_E})\gamma_D}{\bar{\gamma}_E\sqrt{\eta_E\alpha_{2_E}}},\frac{(1-\sqrt{\eta_E\alpha_{2_E}}c_{2_E})\gamma_D}{\bar{\gamma}_E\sqrt{\eta_E\alpha_{2_E}}}\right)d\gamma_D. \quad (70)$$

With the aid of [26, eq. (1.i), 259], the integral of (70) can be expressed in exact closed-form and this completes the poof of (25).

Following the same steps of (25), the proof of I_2^{Asy} and I_3^{Asy} in (26) and (27), respectively, can be accomplished.

APPENDIX F
PROOF OF COROLLARY 2

For the purpose of brevity in proofing (29), the truncation of the infinite series of I_1^{Asy} is provided. Intuitively, one can observe that $F_D^{(3)}(.)$ of (25) is monotonically decreasing with n. Thus, this yields

$$T_{I_1^{Asy}} \leqslant F_D^{(3)}\left(\mu_D+\mu_E+N+1;\frac{\mu_E}{2}-m_E,m_E,m_E;\mu_E+1;1-\eta_E,1-\sqrt{\eta_E\alpha_{2_E}}c_{1_E},1-\sqrt{\eta_E\alpha_{2_E}}c_{2_E}\right) \times\sum_{n=N}^{\infty}\frac{(1)_n(1)_n}{(2)_n n!}(-\bar{\gamma}_E\sqrt{\eta_E\alpha_{2_E}})^n\Gamma(\mu_D+\mu_E+n+1). \quad (71)$$

Following the similar procedure in [34], we have

$$T_{I_1^{Asy}} \leqslant F_D^{(3)}\left(\mu_D+\mu_E+N+1;\frac{\mu_E}{2}-m_E,m_E,m_E;\mu_E+1;1-\eta_E,1-\sqrt{\eta_E\alpha_{2_E}}c_{1_E},1-\sqrt{\eta_E\alpha_{2_E}}c_{2_E}\right) \times\sum_{n=0}^{\infty}\frac{(1)_{n+N}(1)_{n+N}}{(2)_{n+N}(n+N)!}(-\bar{\gamma}_E\sqrt{\eta_E\alpha_{2_E}})^{n+N} \times\Gamma(\mu_D+\mu_E+n+N+1). \quad (72)$$

Invoking the properties $(x)_{a+b} = (x)_a(x+a)_b$ [26, eq. (1.1.20), p. 22], $\Gamma(a+b) = (a)_b\Gamma(a)$ [26, eq. (1.1.15), p. 22], $x! = \Gamma(x+1)$ [26, eq. (1.1.13), p. 21], and $(1)_x = x!$ [26, eq. (1.1.14), p. 21], (72) becomes

$$T_{I_1^{Asy}} \leqslant F_D^{(3)}\left(\mu_D+\mu_E+N+1;\frac{\mu_E}{2}-m_E,m_E,m_E;\mu_E+1;1-\eta_E,1-\sqrt{\eta_E\alpha_{2_E}}c_{1_E},1-\sqrt{\eta_E\alpha_{2_E}}c_{2_E}\right) (-\bar{\gamma}_E\sqrt{\eta_E\alpha_{2_E}})^N\frac{\Gamma(\mu_D+\mu_E+N+1)}{\Gamma(N+1)} \times\sum_{n=0}^{\infty}\frac{(\mu_D+\mu_E+N+1)_n(N+1)_n(1)_n(1)_n(1)_n}{(2)_n(2+N)_n n!} \times(-\bar{\gamma}_E\sqrt{\eta_E\alpha_{2_E}})^n. \quad (73)$$

With the help of [26, eq. (1.4.1), p. 42], (73) can be written in exact closed-form expression as shown in the first term of (29). Similarly, the number of terms of I_2^{Asy} and I_3^{Asy} which represent the second and third terms, respectively, can be deduced. Substituting the results into (24) to obtain (29) and this completes the proof.

APPENDIX G
PROOF OF THEOREM 5

Similar to Theorem 4, plugging $\Phi_2^{(4)}(\frac{\mu_D}{2}-m_D,\frac{\mu_D}{2}-m_D,m_D,m_D;\mu_D+1;0,0,0,0) = 1$ in (49),

we have

$$\begin{aligned}\mathrm{SOP}^{Asy} &\approx \frac{\Omega_D\Omega_E}{\Gamma(\mu_D+1)\Gamma(\mu_E)}\int_0^{\infty}\gamma_E^{\mu_E-1}(\theta\gamma_E+\theta-1)^{\mu_D}\\ &\times\Phi_2^{(4)}\Bigg(\frac{\mu_E}{2}-m_E,\frac{\mu_E}{2}-m_E,m_E,m_E;\mu_E;\\ &-\frac{\gamma_E}{\bar{\gamma}_E\sqrt{\eta_E\alpha_{2_E}}},-\frac{\sqrt{\eta_E}\gamma_E}{\bar{\gamma}_E\sqrt{\alpha_{2_E}}},-\frac{c_{1_E}\gamma_E}{\bar{\gamma}_E},-\frac{c_{2_E}\gamma_E}{\bar{\gamma}_E}\Bigg)d\gamma_E.\end{aligned} \tag{74}$$

The following identity [31, eq. (1.110), p. 25] can be used in (74)

$$(1+a)^b=\sum_{n=0}^{\infty}\binom{b}{n}a^n \tag{75}$$

Consequently, with the aid of (59) and (75) and performing some simple mathematical manipulations, (74) can be rewritten as

$$\begin{aligned}\mathrm{SOP}^{Asy} &\approx \frac{\Omega_D\Omega_E}{\Gamma(\mu_D+1)\Gamma(\mu_E)}\sum_{n=0}^{\infty}\binom{\mu_D}{n}\frac{\theta^n}{(\theta-1)^{n-\mu_D}}\\ &\times\int_0^{\infty}\gamma_E^{\mu_E+n-1}e^{-\frac{\gamma_D}{\bar{\gamma}_E\sqrt{\eta_E\alpha_{2_E}}}}\Phi_2^{(3)}\Bigg(\frac{\mu_E}{2}-m_E,\\ &m_E,m_E;\mu_E;\frac{(1-\eta_E)\gamma_E}{\bar{\gamma}_E\sqrt{\eta_E\alpha_{2_E}}},\frac{(1-\sqrt{\eta_E\alpha_{2_E}}c_{1_E})\gamma_E}{\bar{\gamma}_E\sqrt{\eta_E\alpha_{2_E}}},\\ &\frac{(1-\sqrt{\eta_E\alpha_{2_E}}c_{2_E})\gamma_E}{\bar{\gamma}_E\sqrt{\eta_E\alpha_{2_E}}}\Bigg)d\gamma_E.\end{aligned} \tag{76}$$

Recalling [26, eq. (1.i), p. 259] to express the integral of (76) in exact-closed form and the proof is accomplished.

REFERENCES

[1] A. D. Wyner, "The wire-tap channel," *Bell Syst. Tech. J.*, vol. 54, no. 8, pp. 1355–1387, Oct. 1975.

[2] J. Barros and M. R. D. Rodrigues, "Secrecy capacity of wireless channels," in *Proc. IEEE Int. Symp. Inf. Theory*, Seattle, WA, USA, Jul. 2006, pp. 356–360.

[3] M. Bloch, J. Barros, M. R. D. Rodrigues, and S. W. McLaughlin, "Wireless information-theoretic security," *IEEE Trans. Inf. Theory*, vol. 54, no. 6, pp. 2515–2534, Jun. 2008.

[4] X. Liu, "Probability of strictly positive secrecy capacity of the Rician-Rician fading channel," *IEEE Wireless Commun. Lett.*, vol. 2, no. 1, pp. 50–53, Feb. 2013.

[5] S. Iwata, T. Ohtsuki, and P.-Y. Kam, "Performance analysis of physical layer security over Rician/Nakagami-m fading channels," in *Proc. IEEE Veh. Technol. Conf. (VTC Spring)*, Sydney, NSW, Australia, Jun. 2017, pp. 1–6.

[6] X. Liu, "Probability of strictly positive secrecy capacity of the Weibull fading channel," in *Proc. IEEE Global Commun. Conf. (GLOBECOM)*, Atlanta, GA, USA, Dec. 2013, pp. 659–664.

[7] X. Liu, "Average secrecy capacity of the Weibull fading channel," in *Proc. 13th IEEE Annu. Consum. Commun. Netw. Conf. (CCNC)*, Las Vegas, NV, USA, Jan. 2016, pp. 841–844.

[8] N. Bhargav, S. L. Cotton, and E. David Simmons, "Secrecy capacity analysis over κ–μ fading channels: Theory and applications," *IEEE Trans. Commun.*, vol. 64, no. 7, pp. 3011–3024, Jul. 2016.

[9] H. Lei, I. S. Ansari, G. Pan, B. Alomair, and M.-S. Alouini, "Secrecy capacity analysis over $\alpha-\mu$ fading channels," *IEEE Commun. Lett.*, vol. 21, no. 6, pp. 1445–1448, Jun. 2017.

[10] L. Kong, G. Kaddoum, and D. B. da Costa, "Cascaded α-μ fading channels: Reliability and security analysis," *IEEE Access*, vol. 6, pp. 41978–41992, 2018.

[11] L. Kong, G. Kaddoum, and H. Chergui, "On physical layer security over Fox's H-function wiretap fading channels," Aug. 2018, *arXiv:1808.03343*. [Online]. Available: https://arxiv.org/pdf/1808.03343.pdf

[12] N. Bhargav and S. L. Cotton, "Secrecy capacity analysis for α-μ/κ-μ and κ-μ/α-μ fading scenarios," in *Proc. IEEE 27th Annu. Int. Symp. Pers., Indoor, Mobile Radio Commun. (PIMRC)*, Valencia, Spain, Sep. 2016, pp. 1–6.

[13] J. M. Moualeu, D. B. da Costa, W. Hamouda, U. S. Dias, and R. A. A. de Souza, "Physical layer security over α-κ-μ and α-η-μ fading channels," *IEEE Trans. Veh. Technol.*, vol. 68, no. 1, pp. 1025–1029, Jan. 2019.

[14] A. Mathur, Y. Ai, M. R. Bhatnagar, M. Cheffena, and T. Ohtsuki, "On physical layer security of α-η-κ-μ fading channels," *IEEE Commun. Lett.*, vol. 22, no. 10, pp. 2168–2171, Oct. 2018.

[15] H. Lei, C. Gao, I. S. Ansari, Y. Guo, G. Pan, and K. A. Qaraqe, "On physical-layer security over SIMO generalized-K fading channels," *IEEE Trans. Veh. Technol.*, vol. 65, no. 9, pp. 7780–7785, Sep. 2016.

[16] H. Lei, H. Zhang, I. S. Ansari, C. Gao, Y. Guo, G. Pan, and K. A. Qaraqe, "Performance analysis of physical layer security over generalized-K fading channels using a mixture Gamma distribution," *IEEE Commun. Lett.*, vol. 20, no. 2, pp. 408–411, Feb. 2016.

[17] G. C. Alexandropoulos and K. P. Peppas, "Secrecy outage analysis over correlated composite Nakagami-m/Gamma fading channels," *IEEE Commun. Lett.*, vol. 22, no. 1, pp. 77–80, Jan. 2018.

[18] L. Kong and G. Kaddoum, "On physical layer security over the Fisher-Snedecor F wiretap fading channels," *IEEE Access*, vol. 6, pp. 39466–39472, 2018.

[19] F. J. Lopez-Martinez, J. M. Romero-Jerez, and J. F. Paris, "On the calculation of the incomplete MGF with applications to wireless communications," *IEEE Trans. Commun.*, vol. 65, no. 1, pp. 458–469, Jan. 2017.

[20] J. Sun, X. Li, M. Huang, Y. Ding, J. Jin, and G. Pan, "Performance analysis of physical layer security over κ-μ shadowed fading channels," *IET Commun.*, vol. 12, no. 8, pp. 970–975, May 2018.

[21] H. Al-Hmood and H. S. Al-Raweshidy, "Exact closed-form capacity and outage probability of physical layer security in κ-μ shadowed fading channels," *IET Commun.*, to be published.

[22] P. Ramirez-Espinosa, F. J. Lopez-Martinez, J. F. Paris, M. D. Yacoub, and E. Martos-Naya, "An extension of the κ-μ shadowed fading model: Statistical characterization and applications," *IEEE Trans. Veh. Technol.*, vol. 67, no. 5, pp. 3826–3837, May 2018.

[23] J. Chen and C. Yuan, "Coverage and rate analysis in downlink L-tier HetNets with fluctuating Beckmann fading," *IEEE Commun. Lett.*, to be published.

[24] H. R. Alhennawi, M. M. H. E. Ayadi, M. H. Ismail, and H.-A. M. Mourad, "Closed-form exact and asymptotic expressions for the symbol error rate and capacity of the H-function fading channel," *IEEE Trans. Veh. Technol.*, vol. 65, no. 4, pp. 1957–1974, Apr. 2016.

[25] H. Chergui, M. Benjillali, and M.-S. Alouini, "Rician K-factor-based analysis of XLOS service probability in 5G outdoor ultra-dense networks," Apr. 2018, *arXiv:1804.08101*. [Online]. Available: https://arxiv.org/abs/1804.08101

[26] H. M. Srivastava and H. L. Manocha, *A Treatise on Generating Functions*. New York, NY, USA: Wiley, 1984.

[27] A. M. Mathai, R. K. Saxena, and H. J. Haubold, *The H-Function: Theory and Applications*. New York, NY, USA: Springer, 2009.

[28] J. F. Paris, "Statistical characterization of κ-μ shadowed fading," *IEEE Trans. Veh. Technol.*, vol. 63, no. 2, pp. 518–526, Feb. 2014.

[29] *MATLAB Code for Computing $F^{(n)}{}_D(.)$.* Accessed: Jun. 14, 2019. [Online]. Available: http://faculty.smu.edu/rbutler/

[30] Y. Liu, Z. Qin, M. Elkashlan, Y. Gao, and L. Hanzo, "Enhancing the physical layer security of non-orthogonal multiple access in large-scale networks," *IEEE Trans. Wireless Commun.*, vol. 16, no. 3, pp. 1656–1672, Mar. 2017.

[31] I. S. Gradshteyn and I. M. Ryzhik, *Table of Integrals, Series, and Products*, 7th ed. New York, NY, USA: Academic, 2007.

[32] J. Jung, S.-R. Lee, H. Park, S. Lee, and I. Lee, "Capacity and error probability analysis of diversity reception schemes over generalized-K fading channels using a mixture gamma distribution," *IEEE Trans. Wireless Commun.*, vol. 13, no. 9, pp. 4721–4730, Sep. 2014.

[33] H. Exton, *Multiple Hypergeometric Functions and Applications* (Mathematics and Its Applications). Amsterdam, The Netherlands: Ellis Horwood, 1976.

[34] H. Al-Hmood, "Performance analysis of energy detector over generalised wireless channels in cognitive radio," Ph.D. dissertation, Brunel Univ. London, London, U.K., 2015.

HUSSIEN AL-HMOOD (S'12–M'15) received the B.S. and M.Sc. degrees in electrical and electronic engineering from Baghdad University, Iraq, Baghdad, Iraq, in 2005 and 2007, respectively, and the Ph.D. degree from Brunel University London, London, U.K., in 2015. He is currently an Associate Professor with the Electrical and Electronic Engineering (EEE) Department, University of Thi-Qar, Thi-Qar, Iraq, where he was the Head of the EEE Department, from November 2016 to October 2018. He participated in many international conferences and has published the number of articles in high-quality journals, such as IEEE and IET. His current research interests include estimation and detection techniques, such as energy detection, cognitive radio and cooperative communications networks, diversity combining and MIMO systems, statistical characterizations of generalized composite fading channels, security of physical layer, coexistence techniques between Wi-Fi and LAA, and channel model of mmWave for 5G. In 2017, he received the Fulbright USA Scholar Grant to visit the University of Delaware, Delaware, USA. He has served as a Reviewer for many high-quality journals, such as the IEEE TRANSACTIONS ON VEHICULAR TECHNOLOGY (TVT), the IEEE WIRELESS COMMUNICATIONS LETTERS (WCL), *Electronics Letters*, the IEEE COMMUNICATIONS LETTERS (CL), IEEE ACCESS, and the IEEE TRANSACTIONS ON COMMUNICATIONS (TCOM).

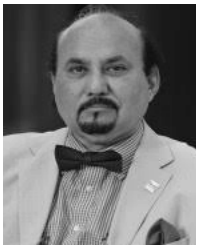

HAMED AL-RAWESHIDY (M'92–SM'97) received the Ph.D. degree from Strathclyde University, Glasgow, U.K., in 1991. He was with the Space and Astronomy Research Centre, Iraq; PerkinElmer, USA; Carl Zeiss, Germany; British Telecom, U.K.; Oxford University; Manchester Metropolitan University; and Kent University. He is currently the Director of the Wireless Networks and Communications Centre (WNCC) and the Director of PG studies (ECE) at Brunel University London, London, U.K. WNCC is the largest center at Brunel University London and one of the largest Communication Research Centre in U.K. He has published over 400 articles in international journals and referred conferences. He is the Editor of the first book *Radio over Fibre Technologies for Mobile Communications Networks*. He acts as a Consultant and involved in projects with several companies and operators, such as Vodafone, U.K.; Ericsson, Sweden; Andrew, USA; NEC, Japan; Nokia, Finland; Siemens, Germany; Franc Telecom, France; Thales, U.K. and France; and Tekmar, Italy. He is a Principal Investigator for several EPSRC projects and European project, such as MAGNET EU project (IP), from 2004 to 2008. His current research interests include 5G and beyond, such as C-RAN, SDN, the IoT, M2M, and radio over fiber.